Cell

Article

Transport mechanism and pharmacology of the human GlyT1

Graphical abstract

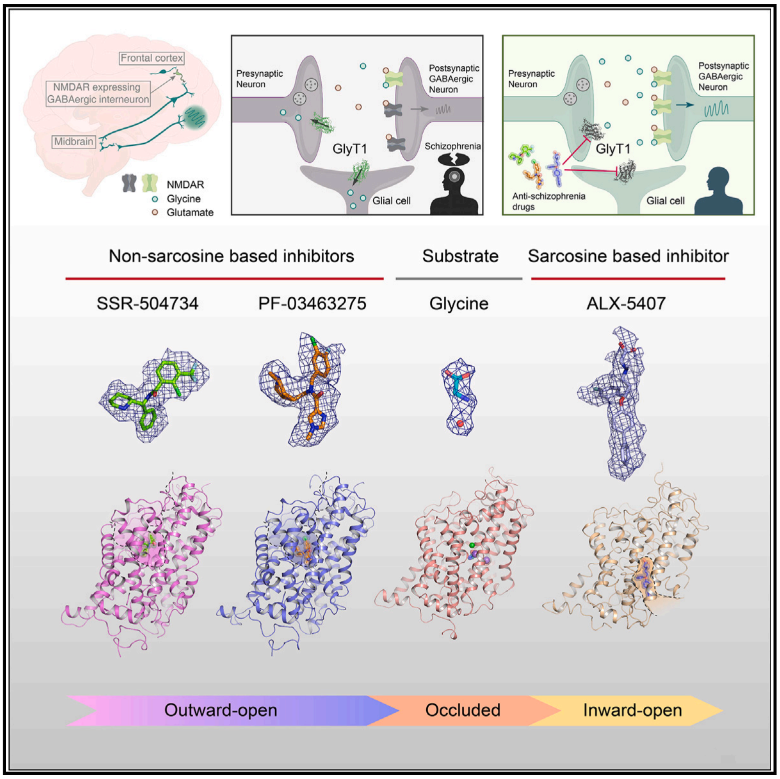

Highlights

- Glycine-bound complex illuminates binding pocket of substrate and Na^+/Cl^- ions
- Sarcosine-based ALX-5407 stabilizes GlyT1 in its inward-facing state
- SSR-504734 and PF-03463275 stabilize outward-facing GlyT1 with varied pockets
- Transport mechanism elucidated by structures in outward, occluded, and inward states

Authors

Yiqing Wei, Renjie Li, Yufei Meng, ..., Qinru Bai, Na Li, Yan Zhao

Correspondence

zhaoy@ibp.ac.cn

In brief

This work reports the structures of human glycine transporter 1 (GlyT1), providing insights on its substrate recognition, conformational transition, and distinct binding pockets for anti-schizophrenia drugs.

Wei et al., 2024, Cell *187*, 1719–1732
March 28, 2024
https://doi.org/10.1016/j.cell.2024.02.026

Cell

CellPress

Article

Transport mechanism and pharmacology of the human GlyT1

Yiqing Wei,[1,5,6] Renjie Li,[1,5,6] Yufei Meng,[1,5,6] Tuo Hu,[1,5,6] Jun Zhao,[3,6] Yiwei Gao,[1,5] Qinru Bai,[1,5] Na Li,[4] and Yan Zhao[1,2,7,*]
[1]Key Laboratory of Biomacromolecules (CAS), National Laboratory of Biomacromolecules, CAS Center for Excellence in Biomacromolecules, Institute of Biophysics, Chinese Academy of Sciences, Beijing 100101, China
[2]State Key Laboratory of Brain and Cognitive Science, Institute of Biophysics, Chinese Academy of Sciences, 15 Datun Road, Beijing 100101, China
[3]Peking University Institute of Advanced Agricultural Sciences, Shandong Laboratory of Advanced Agricultural Sciences at Weifang, Weifang, Shandong 261000, China
[4]Heart Center and Beijing Key Laboratory of Hypertension, Beijing Chaoyang Hospital, Capital Medical University, Beijing 100020, China
[5]College of Life Sciences, University of Chinese Academy of Sciences, Beijing 100049, China
[6]These authors contribute equally
[7]Lead contact
*Correspondence: zhaoy@ibp.ac.cn
https://doi.org/10.1016/j.cell.2024.02.026

SUMMARY

The glycine transporter 1 (GlyT1) plays a crucial role in the regulation of both inhibitory and excitatory neurotransmission by removing glycine from the synaptic cleft. Given its close association with glutamate/glycine co-activated NMDA receptors (NMDARs), GlyT1 has emerged as a central target for the treatment of schizophrenia, which is often linked to hypofunctional NMDARs. Here, we report the cryo-EM structures of GlyT1 bound with substrate glycine and drugs ALX-5407, SSR504734, and PF-03463275. These structures, captured at three fundamental states of the transport cycle—outward-facing, occluded, and inward-facing—enable us to illustrate a comprehensive blueprint of the conformational change associated with glycine reuptake. Additionally, we identified three specific pockets accommodating drugs, providing clear insights into the structural basis of their inhibitory mechanism and selectivity. Collectively, these structures offer significant insights into the transport mechanism and recognition of substrate and anti-schizophrenia drugs, thus providing a platform to design small molecules to treat schizophrenia.

INTRODUCTION

Glycine is a fundamentally important neurotransmitter that performs multiple functions in the central nervous system (CNS).[1,2] Serving as an inhibitory neurotransmitter, it is predominantly active in the brainstem and spinal cord, where it is involved in a broad spectrum of motor and sensory functions.[2–4] However, it also participates in excitatory neurotransmission as an obligatory co-agonist of the NMDA receptors (NMDARs).[5] The synaptic concentration of glycine is primarily regulated by two high-affinity sodium- and chloride-dependent transporters, glycine transporter 1 (GlyT1) (*SLC6A9*)[6] and GlyT2 (*SLC6A5*),[7] which belong to neurotransmitter sodium symporter (NSS) family.[8] These two transporters exhibit a complementary distribution and function within the nervous system.[9–11] Distinct from the GlyT2, which is predominantly expressed in glycinergic nerve terminals,[12,13] the GlyT1 is primarily expressed in astrocytes, as well as in glutamatergic neurons, and is thought to regulate NMDARs activity by impacting the availability of the co-agonist glycine.[14] GlyT1 homozygous knock-out mice develop severe neuromotor deficits leading to premature death, whereas heterozygous GlyT1$^{+/-}$ mice, which display a 50% reduction in the levels of GlyT1 and exhibit impaired glutamatergic function,[15,16] highlighting the critical functional roles of GlyT1 in both inhibitory and excitatory neurotransmission.

Schizophrenia is a severe and chronic mental illness with a prevalence affecting up to 1% of the population.[17] Increasing evidence has shown that the NMDAR plays a pivotal role in the pathophysiology of schizophrenia.[18,19] Remarkably, open-channel blockers of NMDARs can induce schizophrenia-like symptoms in healthy individuals.[20,21] Consequently, enhancing the function of the NMDARs has emerged as a promising therapeutic strategy for treating schizophrenia. Clinical studies have suggested that agonists of the glycine site in the NMDAR, such as glycine and D-serine, could potentially be beneficial in treating schizophrenia.[22,23] As a result, numerous selective GlyT1 inhibitors have been developed aiming at enhancing glycine concentration in synaptic cleft and indirectly augmenting the activity of NMDARs. These GlyT1 selective inhibitors can be categorized into sarcosine-based and non-sarcosine-based inhibitors, based on their chemical structures.[24] Sarcosine, an endogenous inhibitor of GlyT1, does not affect GlyT2.[25,26] Derivatives of sarcosine, such as ALX-5407, can effectively inhibit GlyT1 with high specificity. However, the inhibitory effect of sarcosine-based inhibitors is often irreversible and leads to severe side effects.[27] To circumvent this issue, a variety of non-sarcosine-based derivative inhibitors have been developed, including methylphenidate-derived GlyT1 inhibitors represented by SSR504734,[28,29] heteroaryl amide GlyT1 inhibitors represented by PF-03463275.[30] Drugs from each of these categories are currently undergoing pre-market clinical trials.[31] Even though the crystal structure of GlyT1 bound with Cmpd1 has been determined, it only reveals an inward-facing conformation,[32] leaving a multitude of mechanistic insights yet to be elucidated. These include the molecular mechanisms of substrate glycine recognition, ion binding, and conformational changes during the transport cycle, crucial for understanding the glycine reuptake process in the brain. Additionally, it is essential to explore how various chemical derivatives selectively bind and inhibit GlyT1, critical information for the further rational design of potent, highly specific, and reversible GlyT1 inhibitors to treat schizophrenia.

In this study, we determined structures of GlyT1-bound substrate glycine (GlyT1^{Gly}), sarcosine-based inhibitor ALX-5407 (GlyT1^{ALX}), non-sarcosine-based inhibitors SSR504734 (GlyT1^{SSR}), and PF-03463275 (GlyT1^{PF}). These structures are stabilized in three different conformations, including outward-facing conformation (GlyT1^{SSR}/GlyT1^{PF}), occluded state (GlyT1^{Gly}), and inward-facing conformation (GlyT1^{ALX}), which allow us to establish a blueprint for understanding the transport cycle and inhibitory mechanism of GlyT1. Moreover, with the aid of [^{3}H]glycine uptake assay, we are able to clearly demonstrate the specific structural disparities that allow each inhibitor to discriminate between GlyT1 and GlyT2.

RESULTS

Structural determination and architecture

To investigate the molecular mechanism through which GlyT1 recognizes its substrate, we recombinantly expressed a GFP-tagged full-length and wild-type (WT) GlyT1 using the HEK293 system. Initially, we carried out a [^{3}H]glycine uptake assay. The HEK293 cells expressing GlyT1 demonstrated significant glycine uptake activity when compared with the HEK293 cells used as a negative control (Figure S1A), suggesting that this construct is functional. Further analysis revealed that the GlyT1 tagged with GFP and twin-strepII exhibits an apparent affinity for the substrate glycine that is similar to that of the untagged GlyT1 (Figure S1B). Subsequently, we carried out thermofluor assay to identify detergents that stabilize the GlyT1. We found that the digitonin can enhance the thermostability of the GlyT1 compared with other detergents (Figure S1C). Therefore, we purified it using digitonin detergent and reconstituted it into nanodiscs to determine its structure. The purified sample exhibits a symmetric profile on size-exclusion chromatography (Figure S1D), and the SDS-PAGE shows two prominent bands (GlyT1 and MSP1D1E3) (Figure S1E). The smeared bands above GlyT1 probably due to heterogeneity in the glycosylation. We incubated the purified sample with substrate or inhibitors, and determined the structures of GlyT1 in complex with glycine (GlyT1^{Gly}), ALX-5407 (GlyT1^{ALX}), SSR504734 (GlyT1^{SSR}), and PF-03463275 (GlyT1^{PF}) at resolutions of 2.6, 3.3, 3.2, and 3.0 Å (Figures 1C and S1F–S1M; Table S1), respectively.

The GlyT1 structure, encompassing a width and length of 55 and 60 Å, respectively (Figure 1A), exhibits a classic LeuT fold, akin to other neurotransmitter transporters.[33–38] It comprises 12 transmembrane (TM) helices, with both the N and C termini located at the cytoplasmic side (Figure 1B). The overall folding of GlyT1 presents a pseudo 2-fold symmetry, with the symmetry axis aligned parallel to the plane of the membrane, relating TMs 1–5 to TMs 6–10. In particular, both TM1 and TM6 exhibit characteristic unwinding in the middle, and these unwound segments intersect near the pseudo 2-fold axis. Such disruptions in the helix are likely to contribute to the formation of the ligand-binding pocket. The GlyT1 harbors several extended loops at both extracellular and intracellular sides. For instance, the extracellular loop connecting TM3 and TM4 (EL2) contains residues ranging from H159 to R233. Residues 177–207 have not been determined in the cryoelectron microscopy (cryo-EM) map, presumably due to their high flexibility. A disulfide bond, C166–C175, has been identified within this loop. This disulfide bond is conserved in other neurotransmitter transporters (Figure S2) and is probably important to preserve a specific configuration of the EL2. A previous study has shown that the N-linked glycosylation of GlyT1 is crucial for trafficking of GlyT1 to plasma membrane.[39] However, in our structure, these glycosylation sites could not be determined, likely due to their high flexibility.

Glycine and ion binding of the GlyT1

The glycine and ion binding pockets are situated in a cavity midway through the membrane bilayer and are inaccessible from both the extracellular and intracellular sides (Figures 2A–2D), indicating that the GlyT1^{Gly} structure exists in an occluded state. The binding cavity is constructed from residues on TMs 1, 3, 6, and 8, and it is positioned 18 Å away from the extracellular side of the membrane surface (Figures 2B and 2C). In specific, the residues Y62 on TM1 (Y62^{TM1}), G65^{TM1}, G67^{TM1}, Y142^{TM3}, Y316^{TM6}, G319^{TM6}, W322^{TM6}, and T418^{TM8} encircle the substrate glycine and are likely pivotal in forming a binding pocket for glycine (Figure 2E). The glycine is stabilized through multiple hydrogen bonds with these surrounding residues. Specifically, the amino group of glycine is coordinated through hydrogen bonds with carbonyl oxygen atom on the backbone of residues Y316^{TM6} and S317^{TM6}. We also observed a water molecule forming hydrogen bonds with both amino group of glycine and carbonyl oxygen of Y62^{TM1}, which is likely also important for glycine binding (Figures 2A and 2E). The nitrogen atom the G67^{TM1} backbone forms a hydrogen bond with the carbonyl oxygen atom of glycine. In addition, the hydroxyl oxygen atom of the Y142^{TM3} side chain forms a hydrogen bond with the hydroxyl oxygen atoms of glycine. The [^{3}H]glycine uptake experiment indicated that the Y62A and Y142A mutations impair transporter function (Figure 2I). The kinetic analysis further demonstrates that the Y142A mutant slightly yet significantly alters the apparent affinity to the glycine and its V_{max} is dramatically decreased compared with that of WT GlyT1 (Figure 2J). The residues Y316^{TM6} and W322^{TM6} formed a T-shaped π-π stacking, contributing to the integrity of glycine binding pocket. The mutants Y316A and W322A significantly impaired the activity of GlyT1 (Figure 2I). In GlyT2, the residue

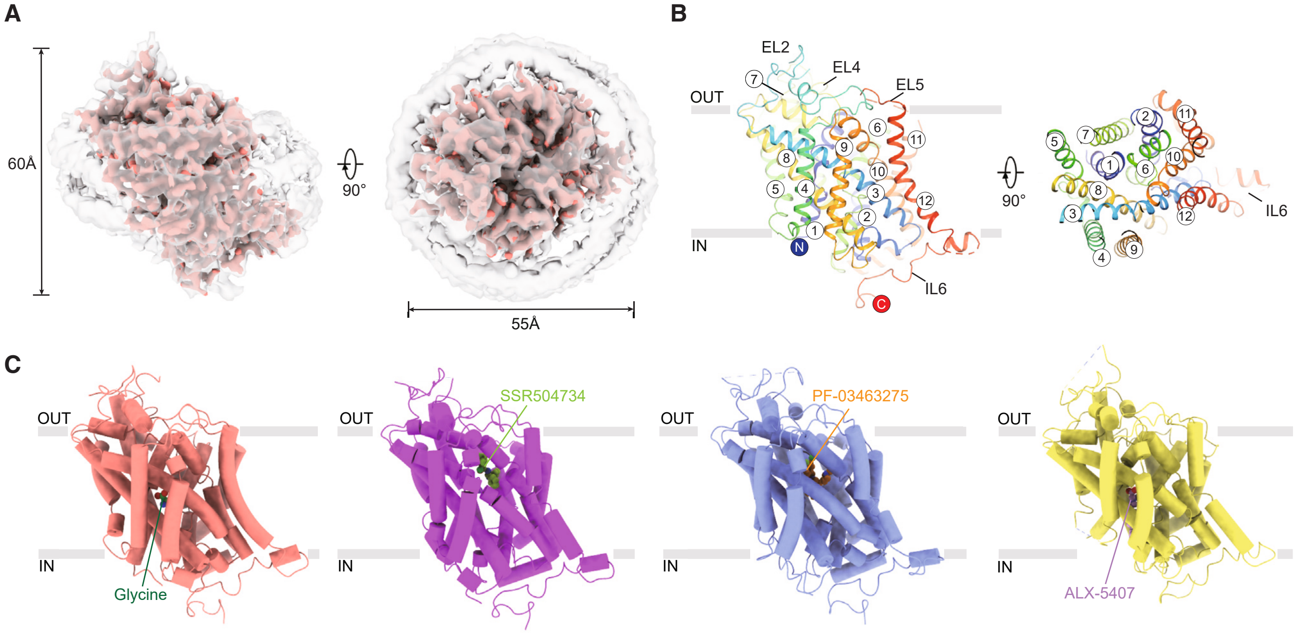

Figure 1. Architecture of the human glycine transporter 1

(A) The cryo-EM maps of representative nanodisc-reconstituted glycine transporter 1 (GlyT1), bound with glycine, viewed in parallel (left) and perpendicular (right) to the membrane. The density of GlyT1 and nanodisc are colored in salmon and gray, respectively. The vertical distance and the diameter of the whole nanodisc are labeled.

(B) Overall structure of GlyT1. N terminus, C terminus, TM1-12, and extracellular/intracellular loops are labeled. The view is consistent with cryo-EM maps in (A).

(C) Overall structures of GlyT1 binding with glycine (GlyT1^{Gly}), SSR504734 (GlyT1^{SSR}), PF-03463275 (GlyT1^{PF}), and ALX-5407 (GlyT1^{ALX}) are represented by salmon, purple, light-blue, and yellow cylinder, respectively.

See also Figure S1.

W482 (abbreviated to W482^{T2}) is equivalent to W322^{TM6} (abbreviated to W322^{T1}) in GlyT1 (Figure S2). A W482R mutation has been identified in a patient with hyperekplexia, effectively eliminating GlyT2 function.[40–42] This provides additional evidence for the essential role of W322^{T1} and W482^{T2} for glycine reuptake. The residues G65^{TM1}, G67^{TM1}, G319^{TM6}, and T418^{TM8}, all of which have small side chains, are involved in the binding pocket (Figure 2E). We speculate that these residues, on the one hand, may be important to provide enough space for the accommodation of glycine. On the other hand, the G67^{TM1} and G319^{TM6}, found at the unwound region of TM1 and TM6, conferring these helices with the flexibility required to transition between various conformations. Replacements of G65A, G67S, and T418Q exhibit a substantial reduction in transport activity of GlyT1 (Figure 2I), probably due to the larger side chains prevent glycine from binding within the pocket. The substitution of G319^{TM6} with serine in GlyT2 at the equivalent position markedly reduces transport activity of GlyT1, yet does not significantly alter K_m for glycine (Figure 2J), suggesting that this mutation does not substantially affect the interaction between the substrate glycine and the transporter. However, the G319L and G319Q mutations completely abolish the transport activity of GlyT1, probably due to the larger side chain causing steric hindrance with the amino group of substrate glycine (Figure 2I). Moreover, GlyT1 is capable of transporting both glycine and sarcosine, whereas GlyT2 is specific to glycine transport. Sarcosine is the N-methyl derivative of glycine, implying that a larger binding pocket is required for GlyT1 compared with GlyT2. In our structural analysis, we observed that the amino terminal of glycine is oriented toward G319^{TM6} within the binding pocket. We hypothesize that the N-methyl group of sarcosine would be positioned proximate to G319^{TM6}. Notably, in GlyT2, G319^{T1} is replaced by serine (S479^{T2}). We observe a water molecule participating in coordination of the amino group of glycine (Figure 2A). We speculate that the hydroxyl group of S479^{T2} might serve a similar role in interacting with amino group of glycine. However, the larger side chain of S479^{T2} would create steric hindrance against sarcosine, thereby rendering GlyT2 incapable of transporting it. The functional study demonstrates that the sarcosine almost completely eliminates glycine uptake activity by GlyT1. Although sarcosine still inhibits the glycine uptake of GlyT1 G319S mutant, its effect is substantially reduced (Figure S3A). Additionally, although GlyT2 is resistant to the sarcosine inhibition, the transport ability of GlyT2 S479G mutant is significantly decreased (Figure S3B). These observations support that the G319^{T1} and S479^{T2} are important for the ability to transport sarcosine through GlyT1 and GlyT2.

The 2.6 Å resolution cryo-EM map allows us to identify the binding sites of these ions. The putative sodium ions are situated within the unwound regions of the of TM1 and TM6, which is consistent with the positions of Na1 and Na2 sites observed in the leucine transporter (LeuT) and serotonin transporter (SERT).[33] Na1 formed six coordination bonds with surrounding residues, including the side chains of N68^{TM1}, N349^{TM7}, S317^{TM6}, and carbonyl oxygen on backbone of residues A63^{TM1} and S317^{TM6} (Figure 2F). Moreover, the Na1 is positioned adjacent to the substrate glycine with a distance of 2.7 Å between Na1 and carboxyl oxygen of glycine.

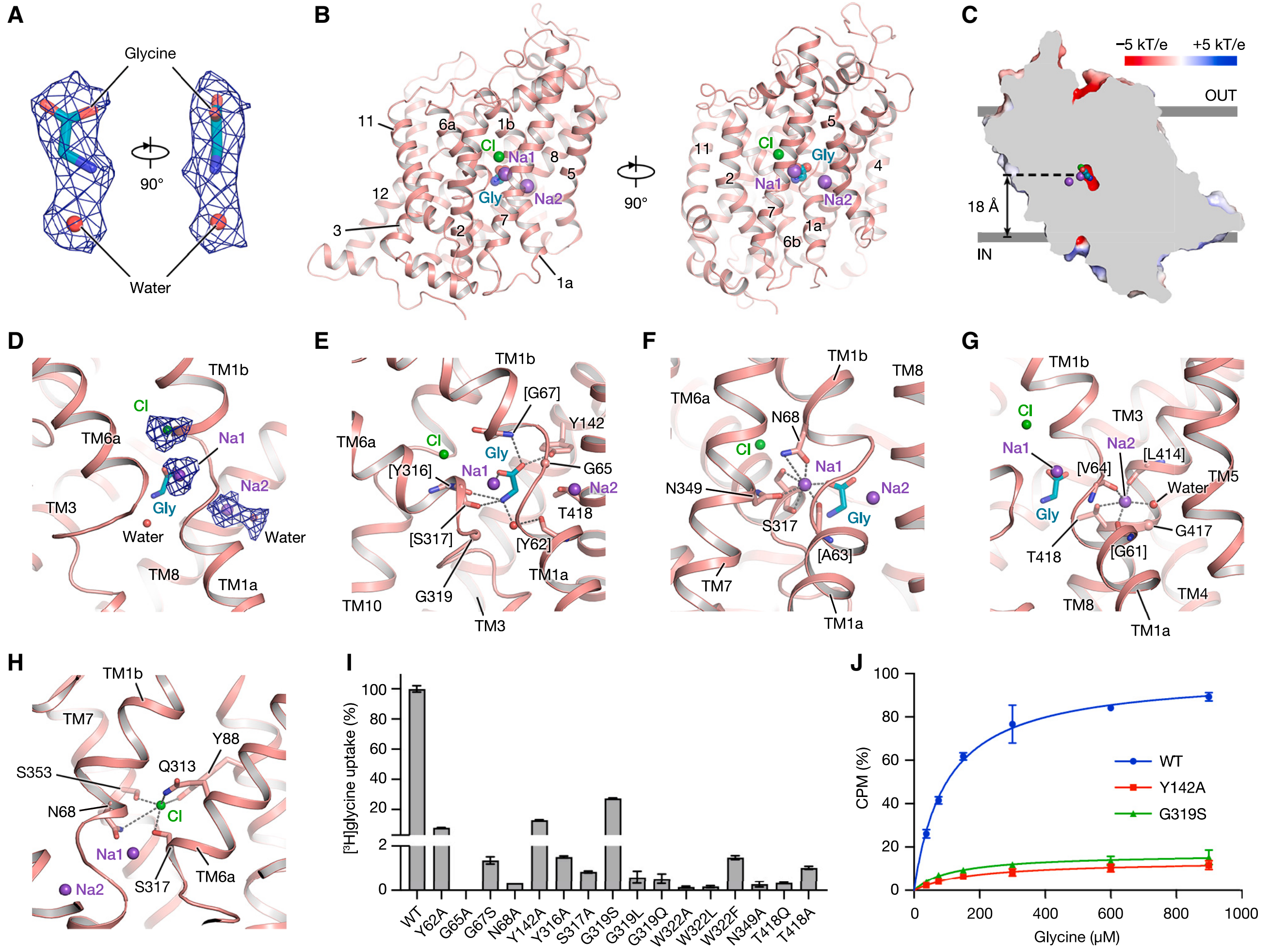

Figure 2. Substrate and ion recognition of GlyT1 in an occluded state

(A) The glycine (cyan sticks) and its coordinated water molecule (red sphere), overlaid with their corresponding EM density (blue mesh).

(B) Overall structure of GlyT1^{Gly} shown as a cartoon, illustrating the binding position of the glycine and ions. The glycine, sodium (Na1 and Na2), and chloride ions are shown as cyan, purple, and green spheres, respectively, and labeled. Transmembrane helices are also labeled.

(C) Electrostatic surface potential of the GlyT1^{Gly}, shown in a slice view through the binding pocket of glycine. The glycine and ions are shown as spheres. The binding pocket of the substrate glycine is negatively charged and located ~18 Å above the inner surface of cell membrane.

(D) Corresponding cryo-EM density of Na1, Na2, and chloride ions, and the water molecule coordinated with Na2, shown as blue mesh and labeled.

(E–H) Zoomed-in view of the binding pocket and interactions of the glycine (E) and ions, namely Na1 (F), Na2 (G), and Cl (H). The glycine is shown as cyan sticks. Sodium (Na1 and Na2) and chloride ions were shown as purple and green spheres, respectively. Water molecules are shown as red spheres. Critical residues interacting with the ligands are shown as sticks and labeled.

(I) Transport activity of GlyT1 WT and mutants quantified using [^{3}H]glycine uptake assay. The transport activity of each mutant is normalized to that of WT GlyT1. The uptake duration is 1 min to ensure the uptake occurs within the linear range. Background uptake of [^{3}H]glycine was subtracted from all groups. Data represent mean ± SEM (error bars), n = 3.

(J) Concentration-dependence of [^{3}H]glycine uptake by HEK293F cells expressing wild-type GlyT1 (blue), mutants Y142A (red), and G319S (green). The transport activities of these two mutants are normalized against the WT GlyT1. Data in curve are obtained from three biologically independent experiments and are presented as mean ± SEM (error bars). K_m values of WT GlyT1, Y142A, and G319S are 101.6 ± 10.86, 178.5 ± 1.67, and 135.6 ± 46.80 μM, respectively. The K_m value of Y142A is significantly different from that of WT GlyT1 ($p = 0.0022$), whereas the K_m values G319S mutant and WT GlyT1 show no statistically significant difference ($p = 0.5183$). Statistical significance was determined using unpaired t tests with alpha = 0.05.

See also Figures S2, S3, and S6.

Therefore, we speculate that the Na1 plays a crucial role in coordinating glycine, and vice versa. The Na2 is located about 6 Å away from the glycine and establishes interactions with the main-chain carbonyl oxygen of G61, V64, and L414, the side-chain hydroxyl oxygen of T418^{TM8}, and a water molecule (Figure 2G). Additionally, we also identified a putative chloride ion binding site. This chloride ion is nestled within a hydrophilic pocket, situated closer to the extracellular side of the membrane plane compared with the glycine binding pocket. In particular, residues including N68^{TM1}, Y88^{TM2}, Q313^{TM6}, S317^{TM6}, and S353^{TM7} coordinate this putative chloride ion (Figure 2H). A previous study indicated that mutations Q313 and S353, involved in chloride binding dramatically decrease

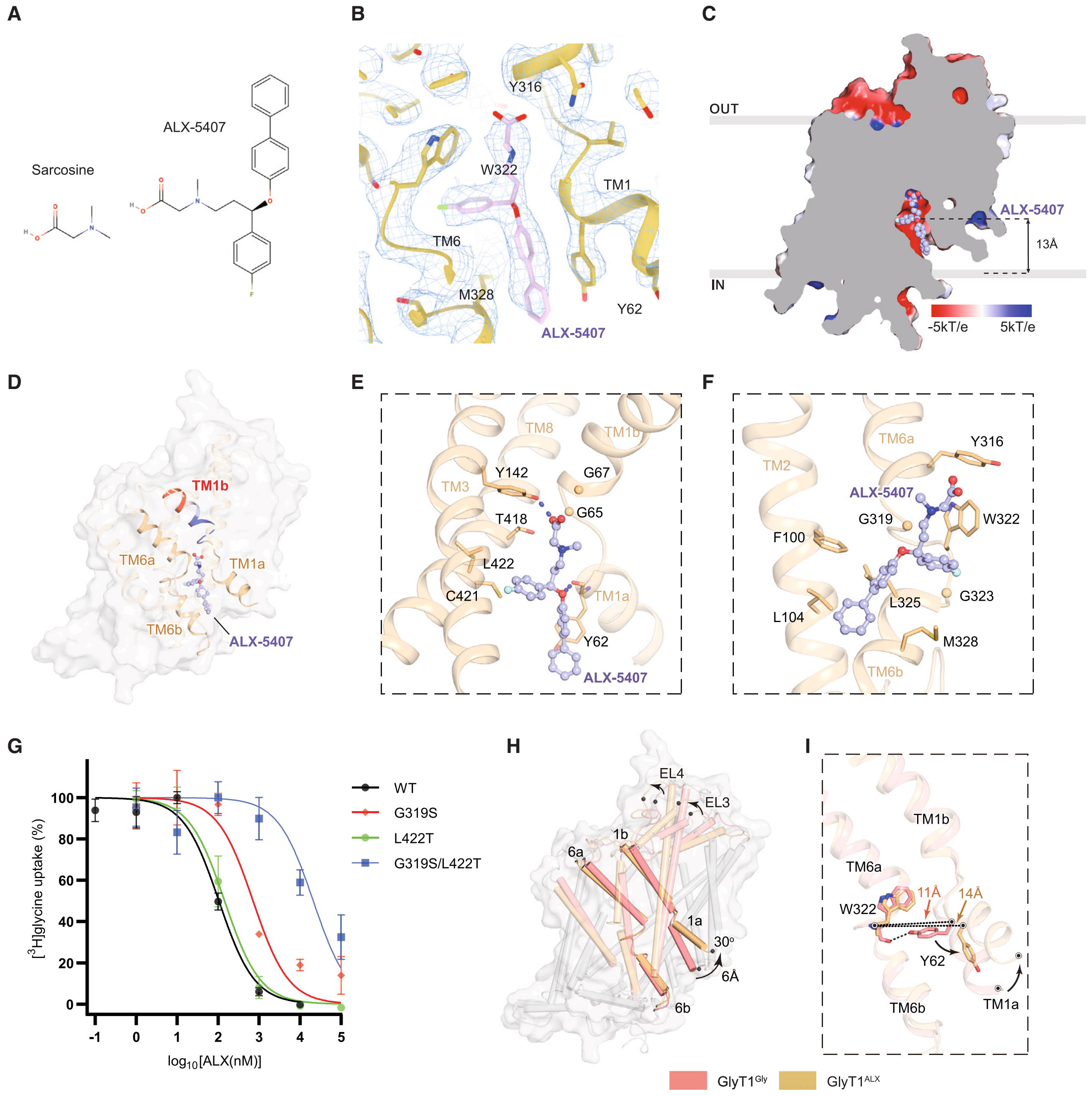

Figure 3. ALX-5407 binding pocket in inward-open state

(A) Chemical structure of sarcosine and ALX-5407.

(B) Cryo-EM density (cyan mesh) and model of ALX-5407 (light-purple sticks) binding pocket.

(C) Sagittal slice through an electrostatic surface potential of GlyT1. The vertical distance from ALX-5407 (light-purple sphere) to cytoplasmic membrane plane is labeled.

(D) GlyT1^{ALX} is displayed as gray surface. The carboxyl terminal of TM1b is colored by red, and amino terminal is colored by blue. The oxygen and nitrogen atom of ALX-5407 are colored by red and blue, respectively.

(E and F) Interaction of ALX-5407 in binding pocket. The key residues for interaction are showed as sticks. The potential hydrogen bond is represented as dashed lines.

(G) Effect of mutations on inhibitory potency of ALX-5407. Specified concentrations of ALX-5407 for WT GlyT1 are in the range of 0.1 nM to 10 μM, whereas for other mutants are 1 nM to 100 μM. Each point represents mean ± SEM (error bars), n = 3. The [^{3}H]glycine uptake has been normalized to cells without inhibitor treatment. WT and mutants are represented by specific symbols and lines defined in the legend.

(legend continued on next page)

glycine influx by GlyT1.[43] Both N68^{TM1} and S317^{TM6} are involved in coordination of Na1 and chloride ion (Figures 2F and 2H). To validate the functional role of these residues within the ion binding sites, we designed a series of mutations, including N68A, S317A, N349A, and T418A. [^{3}H]glycine uptake experiments showed that these mutations almost completely abolish transport activity of GlyT1 (Figure 2I), supporting their functional role in coordinating sodium and chloride ions.

We found that most of these residues involved in glycine binding are conserved in GlyT2 transporter, but they are not strictly conserved in the NSS transporters that uptake neurotransmitters other than glycine (Figure S2). In specific, we compared GlyT1 structure to three other substrate-bound structures of NSS transporters, including drosophila dopamine transporter (dDAT), SERT, and GABA transporter 1 (GAT1).[35,38,44] We found that the substrates glycine, dopamine, serotonin, and GABA were all bound within pockets at similar vertical depths relative to the cytoplasmic membrane plane (Figures S3D–S3G). To understand structural basis of substrate selectivity, we aligned the substrate-binding pocket of GlyT1 with those of dopamine, serotonin, and GABA (Figures S3C–S3G). Given that the serotonin and dopamine are positively charged neurotransmitters, the D98 and D46 within the binding pockets of SERT and dDAT play an essential role in recognizing the amine group. By contrast, this position in GlyT1 is occupied by G65^{TM1} (Figures S3E and S3F). Additionally, W322^{T1} corresponds to F325 in dDAT, F341 in SERT, and L300 in GAT1. This W322^{T1} exhibits obvious clashes with other substrates, including dopamine, serotonin, and GABA (Figures S3E–S3G). The W322F and W322L mutants exhibit only marginal transport (Figure 2I), in line with a previous study demonstrating that mutating of W482^{T2} (equivalent to W322^{T1}) to leucine and phenylalanine leads to a substantial reduction in ability of GlyT2 to transport glycine; however, these two mutations in GlyT2 enable it to transport a wider range of substrates, such as alanine, leucine, and methionine.[40] Therefore, we hypothesize that the larger side chain of W322^{TM6} plays a pivotal role in creating a compact pocket to snugly accommodate the smaller substrate glycine.

We also compared the ion binding sites in GlyT1 with those in LeuT and SERT[33,44] (Figures S3H–S3L). Unlike the carboxyl groups of glycine and leucine that participate in Na1 binding in GlyT1 and LeuT, serotonin, the substrate in SERT, does not interact with Na1. In SERT, D98 is responsible for coordinating Na1, whereas in GlyT1 and LeuT, this position is occupied by glycine (Figures S3H and S3I). Regarding the Na2 binding site, D437 in SERT and T354 in LeuT contribute to the coordination (Figures S3J–S3K). By contrast, in GlyT1, G417, which does not interact with Na2, occupies this position, and we observe an interaction with a water molecule (Figures 2D and 2G). It is worth noting that in other NSS transporters, including GlyT2, the G417 in GlyT1 is replaced by aspartic acid (Figure S3J), suggesting a specific binding mode for Na2 in GlyT1. Although Na1 and Na2 coordination between GlyT1 and SERT shows minor differences, their chloride binding sites are highly conserved (Figure S3L).

Non-competitive inhibition of sarcosine derivative ALX-5407

Sarcosine is an N-methylated derivative of glycine, selectively inhibits GlyT1 over GlyT2.[25,45,46] A series of chemical compounds have been designed and synthesized using sarcosine as a starting point to selectively inhibit the GlyT1.[47] The ALX-5407, also known as (+)-NFPS ((R)-(N-[3-(4′-fluorophenyl)-3-(4′-phenylphenoxy)propyl])sarcosine)), is the "prototypical" sarcosine-derived GlyT1 inhibitor. It potently and non-competitively inhibits GlyT1 but has little inhibitory effect on GlyT2.[27,48,49] We determined the complex structure of GlyT1 with ALX-5407 at a resolution of 3.3 Å (Figure S1G). A three-branched density was observed near the intracellular side, which is well in agreement with the structure of ALX-5407 molecule (Figure 3B).

The ALX-5407 is primarily composed of sarcosine, phenylphenoxy, and fluorophenyl groups (Figure 3A). In our structure, we observed that it extends into a pocket opening toward the cytoplasmic side (Figure 3C). The residues involved in glycine binding at occluded state, including Y316^{TM6}, G319^{TM6}, and W322^{TM6}, are exposed to the cytosol, suggesting that the ALX-5407 stabilizes the GlyT1 at the inward-facing conformation. Given that it attaches within the intracellular cavity, the ALX-5407 manifests a non-competitive inhibitory effect, in line with previous functional studies.[27,49] The carboxyl group of the sarcosine group reaches the bottom of the cavity, approximately 13 Å deep, whereas the phenylphenoxy group is located at the mouth of the cavity (Figure 3C). In specific, the carboxyl group is positioned proximal to the N termini of the TM1b, forming a charge-dipole interaction (Figure 3D). Such an interaction is potentially crucial for binding of all sarcosine derivatives. Given that sarcosine bears a very similar chemical structure to glycine, the binding pattern of the sarcosine group of ALX-5407 might mirror the binding mode of the substrate glycine or sarcosine in the inward-facing state. The carbonyl groups of Y62^{TM1} and hydroxy group of Y142^{TM3} interact with ALX-5407 by forming hydrogen bonds (Figure 3E). Moreover, the fluorophenyl group is surrounded by residues from TM6 and TM8 through van der Waals forces or hydrophobic interactions, including W322^{TM6}, T418^{TM8}, C421^{TM8}, and L422^{TM8} (Figures 3E and 3F). Furthermore, the phenylphenoxy group engaged with GlyT1 through forming extensive hydrophobic interactions with surrounding residues, including Y62^{TM1}, F100^{TM2}, L104^{TM2}, L325^{TM6}, and M328^{TM6} (Figures 3E and 3F). These broad and extensive interactions potentially account for the high affinity and irreversible nature of its blocking effects. The structure of the GlyT1^{ALX} is further compared with previously reported GlyT1 bound to Cmpd1 (Figures S4A–S4C and S4E). The sarcosine-based ALX-5407 and non-sarcosine-based Cmpd1 both occupy a similar binding pocket and align very well (Figure S4E). These structural insights into molecules with distinct functional groups binding to a similar pocket offer valuable information for further drug optimization to enhance their potency, specificity, and reversibility.

(H) Comparison of the occluded (GlyT1^{Gly}, salmon) and inward-open (GlyT1^{ALX}, light-orange) conformations. Critical TMs are represented by colored cylinder, and others are represented by gray. GlyT1^{ALX} is depicted as gray surface. The conformational changes from occluded state to inward-open state are labeled.
(I) GlyT1^{Gly} and GlyT1^{ALX} are represented by salmon and light-orange cartoon, respectively. The distance of Cα from residue Y62 to residue W322 is labeled.
See also Figures S2 and S6.

Previous studies have demonstrated that sarcosine derivatives selectively inhibit GlyT1, as opposed to GlyT2.[50] We found that most of the residues involved in forming the ALX-5407 binding site are conserved between GlyT1 and GlyT2, with G319 as an exception (Figure S2). In GlyT2, G319 is replaced by S479 (S479^{T2}). G319^{T1} is situated on TM6, in proximity to the sarcosine group. Our structure reveals that although G319^{T1} does not appear to directly interact with ALX-5407, its small side chain may be critical in providing adequate space to accommodate ALX-5407 within GlyT1. We speculate that its substitution by serine in GlyT2 probably causes steric hindrance, thus preventing GlyT2 from binding with this inhibitor. Moreover, the L422^{TM8} is located at opposite side of the G319^{TM6}. It is substituted by the T582 in GlyT2. Despite that the side chain of L422^{TM8} is not oriented toward ALX-5407, we speculated that such a replacement causes local conformational change of the TM8, due to alterations in environmental hydrophilicity and volume of the side chain. To validate our hypothesis, we measured the IC_{50} values of ALX-5407 for WT GlyT1 as well as for the G319S, L422T, and G319S/L422T mutants. In our assays, the IC_{50} of ALX-5407 for the WT GlyT1 is approximately 0.1 μM. The L422T mutants show an IC_{50} comparable to that of WT GlyT1, whereas the G319S exhibits significantly reduced sensitivity to ALX-5407, with an IC_{50} value of 0.7 μM (Figure 3G). The double-mutant G319S/L422T further decreases the inhibitory effect of ALX-5407 (IC_{50} of 20.9 μM), indicating that the residue variations in positions G319^{T1} and L422^{T1} serve as key structural elements enabling the selective inhibition of GlyT1 by ALX-5407. This is also consistent with the role of G319 as a critical factor in differentiating the ability of GlyT1 and GlyT2 to uptake sarcosine.

To understand conformational transition from the occluded state to the inward-facing state, we compared structures of GlyT1^{Gly} and GlyT1^{ALX}, resulting in an RMSD value of 1.5 Å over 490 Cα atoms. These two structures are extensively superimposable, with the majority of TM helices exhibiting good alignment (Figure 3H). Even the glycine and sarcosine group of the ALX-5407 are well aligned (Figure S4F), supporting the speculation that the binding pocket of sarcosine group of ALX-5047 is similar to that of glycine when GlyT1 in inward-facing state. However, the TM1a shows substantial structural disparity (Figure 3H). The hydroxyl group of Y62^{TM1} forms a hydrogen bond with W322^{TM6} (Figure 3I). In transition to inward-facing conformational state, the TM1a becomes more extended, elevated by 30°, and shifted by 6 Å (Figure 3H), thereby opening up the cavity toward the cytosol. The residues involved in glycine binding undergo significant conformational changes. The interactions between Y62 and W322 are completely abolished (Figure 3I), with Cα distance changing from 11 Å in the occluded state to 14 Å in the inward-facing state. The side chain of conserved residue Y62 exhibits the most pronounced displacement, flipping by 180°, and consequently exposing the substrate-binding pocket to the cytosol (Figure 3I).

Antagonism of GlyT1 by methylphenidate-derived SSR504734

The SSR504734 (2-chloro-3-(trifluoromethyl)-N-((S)-phenyl((S)-piperidin-2-yl)methyl) benzamide hydrochloride) is a potent, selective, and reversible inhibitor of GlyT1, which is the first patented GlyT1 inhibitor that does not derive from sarcosine to treat schizophrenia.[28,47] Derived from *threo* methylphenidate, it contains a 2-chloro-3-trifluoromethyl, a phenyl, and a piperidinyl, together linked by carboxamide. We determined the GlyT1 structure in complex with SSR504734 at 3.2 Å resolution (Figure S1H). Our structure revealed that the SSR504734 is bound to a pocket that is connected to the extracellular solvent environment, whereas the intracellular gate is closed, indicating that GlyT1^{SSR} is in an outward-facing conformational state (Figure 4C). When we assessed the binding pose of the SSR504734, we found it is surrounded by TM1, TM3, TM6, and EL4 (Figure 4B). The chlorotrifluoromethyl phenyl group is oriented toward the extracellular side, adjacent to W70^{TM1}, V145^{TM3}, P383^{EL4}, L470^{TM10}, and L471^{TM10}. The W70^{TM1} and D474^{TM10} form two hydrogen bonds interaction with the carbonyl oxygen and nitrogen on the carboxamide group (Figure 4D). The piperidine group point toward TM6, stabilized by R71^{TM1} and Q313^{TM6}. The phenyl group forms hydrophobic interactions with I138^{TM3}, Y141^{TM3}, and W322^{TM6} (Figure 4D).

The residues within the SSR504734 binding pocket are not strictly conserved between GlyT1 and GlyT2 (Figure S2). Specifically, the residues V145^{TM3}, L470^{TM10}, and L471^{TM10}, located near the chlorotrifluoromethyl phenyl group of SSR504734 in GlyT1, are substituted by I290, F629, and Q630 in GlyT2, respectively. We hypothesize that these variations in GlyT2, on the one hand, may directly clashes with SSR504734. On the other hand, the L471^{TM10} is replaced by Q630^{T2} may cause change in hydrophobic property of the SSR504734 binding pocket in GlyT2 and consequently lead to the resistant of GlyT2 to the SSR504734. To evaluate this hypothesis, we engineered several mutations, including V145I, L470F, and L471Q, and assessed their response to SSR504734. The [^{3}H]glycine uptake experiment revealed an IC_{50} of 0.19 μM for SSR504734 in the WT GlyT1. However, the IC_{50} values of the V145I, L470F, and L471Q mutant to SSR504734 are 0.44, 0.85, and 0.40 μM (Figure 4E), which all represent reduced affinity compared with WT GlyT1 but do not completely eliminate inhibition. Therefore, we generated a V145I/L470F/L471Q triple mutant. It turns out that the IC_{50} of SSR504734 triple mutant is ~1.3 μM (Figure 4E), almost ~7-fold more than WT GlyT1. However, it still does not match the insensitivity of SSR504734 to GlyT2. We speculate that beyond sequence variations within the binding pocket, variations in residues over a broader spatial range lead to slight yet significant displacement of the TM helices of GlyT2 relative to those in GlyT1. These local conformational changes in TM helices likely alter the shape of the vestibule, resulting in insensitivity of GlyT2 to SSR504734.

To understand inhibitory effect of SSR504734 on GlyT1, the GlyT1^{SSR} structure is superimposed on the GlyT1^{Gly} in the occluded state (Figures S5A and S5B). We found that although the SSR504734 does not directly clash with the substrate glycine, the inhibitor binding disrupts the integrity of substrate-binding site through a subtle displacement of the TM helices surrounding glycine and by altering side-chain orientation of Y316 (Figures S5A and S5B). The residue Y316 is critical for transport activity, as evidenced by Y316A mutation results in significant reduction in transport activity of GlyT1 (Figure 2I). Transport kinetic studies, carried out in the presence of varying

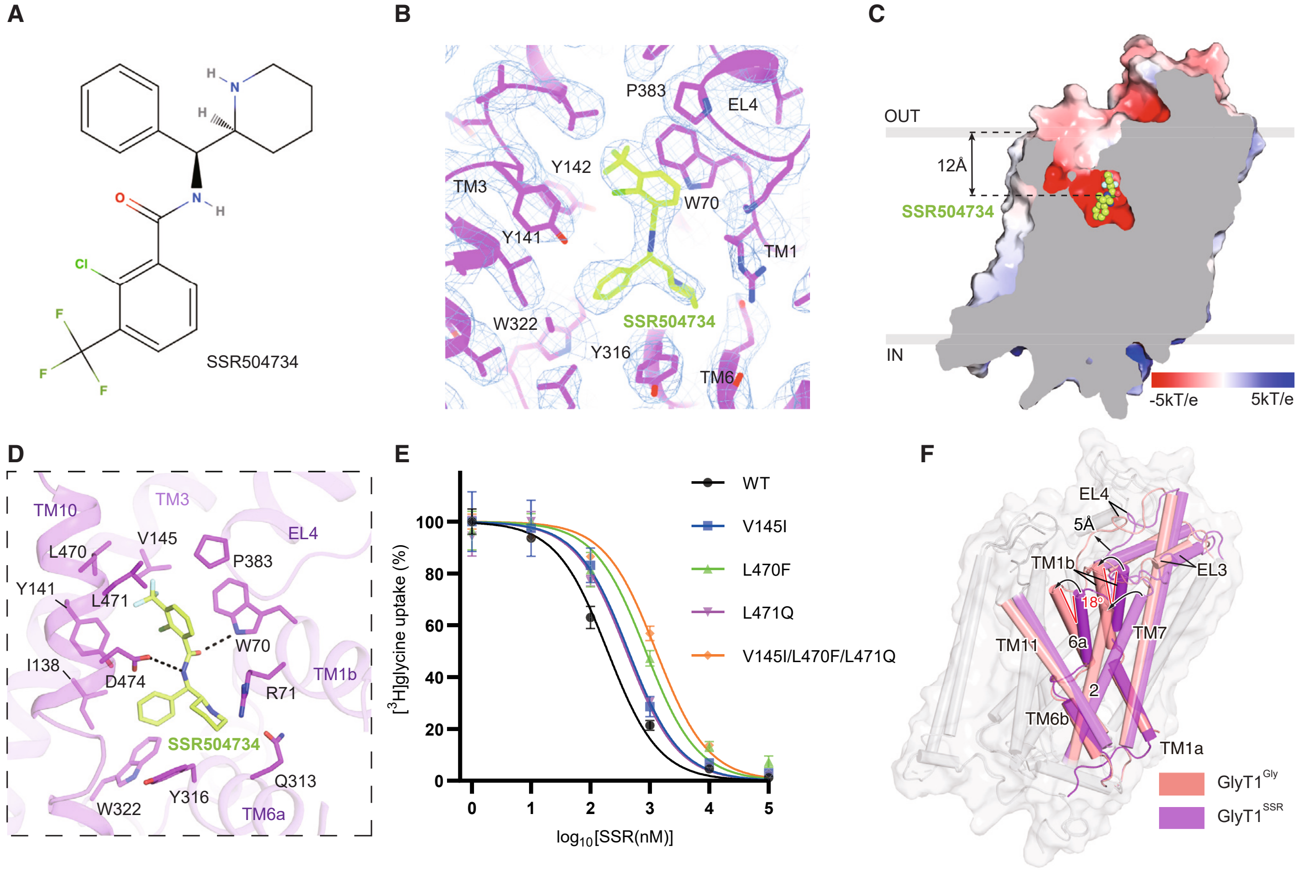

Figure 4. SSR504734 binding site in outward-open conformation

(A) Chemical structure of SSR504734.

(B) Cryo-EM density (cyan mesh) and model of SSR504734 (light-green sticks) binding pocket.

(C) Sagittal slice through an electrostatic surface potential of GlyT1^{SSR}. The vertical distance from SSR504734 (light-green sphere) to cytoplasmic membrane plane is labeled.

(D) Interaction of SSR504734 in binding pocket. The key residues for interaction are showed as sticks. The potential hydrogen bonds are represented as dashed lines.

(E) The inhibition curves of wild-type GlyT1 and various mutants by SSR504734 in the [^{3}H]glycine uptake assay. Specified concentrations of SSR504734 for WT GlyT1 and mutants are in the range of 1 nM to 100 μM. Each point represents mean ± SEM (error bars), n = 3. The [^{3}H]glycine uptake has been normalized to cells without inhibitor treatment. WT and mutants are represented by specific symbols and lines defined in the legend.

(F) Comparison of the occluded (GlyT1^{Gly}, salmon) and outward-open (GlyT1^{SSR}, purple) conformations. Critical TMs are represented by colored cylinder, and others are represented by gray cylinder. Gray surface depicts GlyT1^{SSR}. The conformational changes from occluded state to outward-open state are labeled.
See also Figures S2, S5, and S6.

concentration of SSR504734, reveal a significant increase in the K_m whereas the V_{max} remained relatively unaltered (Figure S5C). These observations suggest that the SSR504734 acts as a competitive inhibitor, in line with a previous report.[27] Moreover, although the majority of the TM helices are nearly identical, a few of them, specifically TM1, TM6, TM7, TM11, and EL4, demonstrate substantial rearrangement (Figure 4F). In the glycine-bound occluded state, TM1b and TM6a lean toward TM8 and TM10 (Figure 5A), effectively sealing off the substrate pathway to the central binding site from the extracellular side. The salt bridge between R71^{TM1} and D474^{TM10} likely plays a pivotal role in knitting these two helices together. Moreover, the residue R71^{TM1} forms a hydrogen bonds with Q313^{TM6} and a cation-π interaction with Y316^{TM6}. The D474^{TM10} establishes hydrogen bonds with hydroxyl groups of residues Y74^{TM1} and Y141^{TM2} (Figure 5B). During the transition to the outward-facing state, TM1b and TM6a diverge from TM8 and TM10, resulting in changes of 18° in their relative angles between these two states (Figure 4F), with the Cα distance between R71^{TM1} and D474^{TM10} shifting from the 10 to 14 Å (Figures 5B and 5C). Additionally, hydrogen bonds and cation-π interactions involving the side chains of R71 and D474, observed in the occluded state, are disrupted (Figure 5C), supporting that these interactions may be important for sealing the extracellular cavity. We designed several mutants, including R71A, R71K, D474E, D474A, and R71D/D474R double mutant. The conservative mutations, such as R71K and D474E, retain approximately 5%–7% of the transport activity compared with that of WT GlyT1. The other mutants

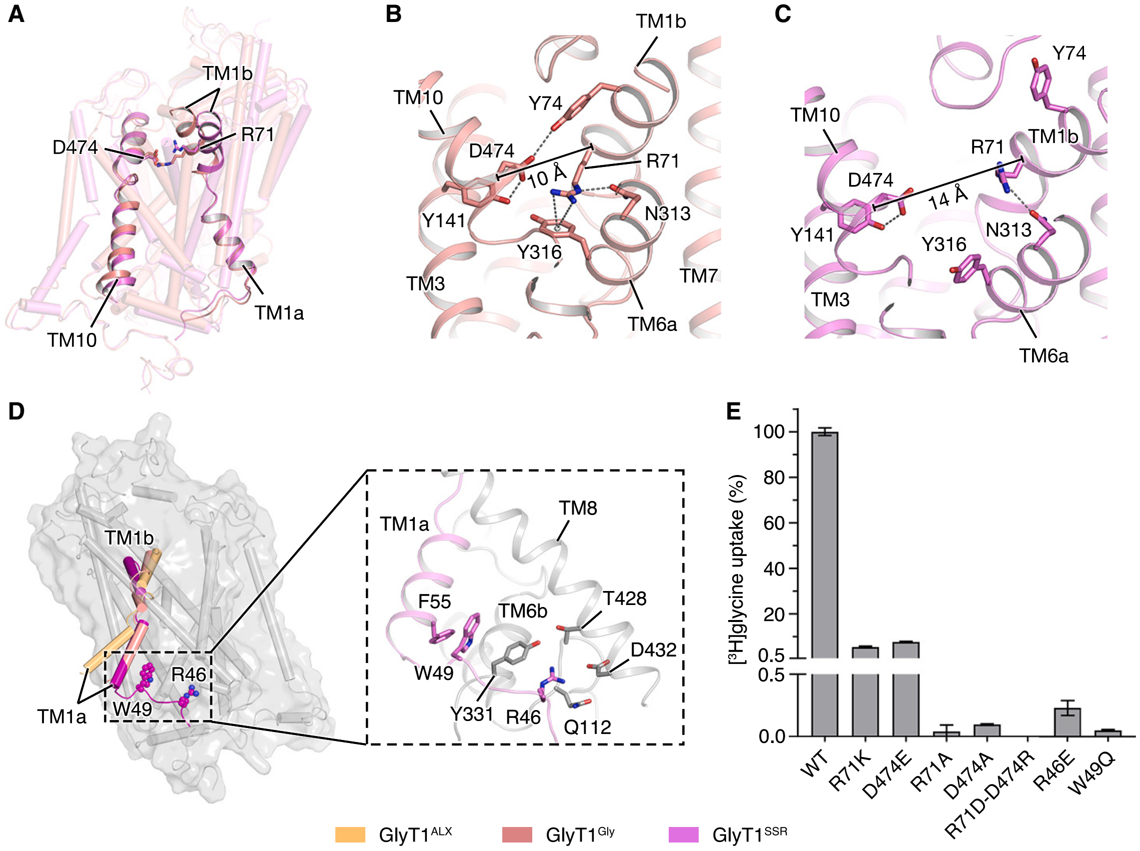

Figure 5. Interactions stabilizing distinct conformations

(A) Alignment of GlyT1^{Gly} (occluded) and GlyT1^{SSR} (outward-open) with scaffold domain. Critical TMs of GlyT1^{Gly} and GlyT1^{SSR} are represented by salmon and pink cartoon, respectively. Other TMs are represented by cylinder. Pivotal residues are represented by sticks.

(B and C) Key residues are displayed as sticks, and interactions are represented by dashed lines in GlyT1^{Gly} (salmon) and GlyT1^{SSR} (pink). Distance between Cα of R71 and D474 are labeled.

(D) Comparison of the N-terminal of GlyT1^{Gly}, GlyT1^{ALX}, and GlyT1^{SSR}. The TM1a and N-terminal of GlyT1^{Gly}, GlyT1^{ALX}, and GlyT1^{SSR} are represented by salmon, light-orange, and pink cylinder, respectively. (Inset) The interactions of N-terminal in outward-open GlyT1. GlyT1^{SSR} is represented by pink cartoon. Key residues are represented by sticks and labeled.

(E) Transport activity of WT and mutants measured by [^{3}H]glycine uptake assay. The transport activity of each mutant is normalized to that of WT GlyT1. The uptake duration is 1 min to ensure the uptake occurs within the linear range. Background uptake of [^{3}H]glycine was subtracted from all groups. Data represent mean ± SEM (error bars), n = 3.

See also Figure S6.

demonstrate minimal glycine uptake activity (Figure 5E). These observations indicate that the salt bridge between R71 and D474, as well as interactions of these two residues with nearby residues, are important for function of GlyT1. Consequently, EL4 in the outward state dips toward the membrane plane by about 5 Å (Figure 4F). The rearrangements of TM1a, TM6, and EL4 lead to minor displacements in adjacent structural elements, including residues Y74^{TM1}, Y316^{TM6}, and Q313^{TM6} (Figures 5B and 5C). Moreover, the N-terminal residues ranging from L44 to Q52 were resolved below the transmembrane domain (TMD) in the outward-facing GlyT1^{SSR} structure. We observed that residue R46 potentially forms an electrostatic interaction with D432^{TM8} and establishes a cation-π interaction with Y331^{TM6} (Figure 5D). Residue W49 engages in the hydrophobic interactions with F55^{TM1} and Y331^{TM6} (Figure 5D). However, this segment was not resolved in inward-facing states. Considering the direct connection of the N-terminal segment with TM1a, we speculate that the interaction between the N-terminal segment and TMD is critical for stabilizing the transporter in its outward-facing and occluded states. The association and dissociation of the N-terminal segment from the TMD might be pivotal for conformational transition and transport activity. Supporting our hypothesis, the R46E and W49Q mutants display negligible activity (Figure 5E).

The structures of GlyT1 are determined in outward-facing, occluded, and inward-facing states, representing three critical functional states in the transport cycle. Similar conformations have been determined for SERT in previous studies.[44,51] We compared the structures of GlyT1 and SERT in each conformational state (Figures S6A–S6C). Throughout these states, the TM helix arrangements of both transporters are almost identical, with only minor displacements (Figures S6D–S6F), suggesting

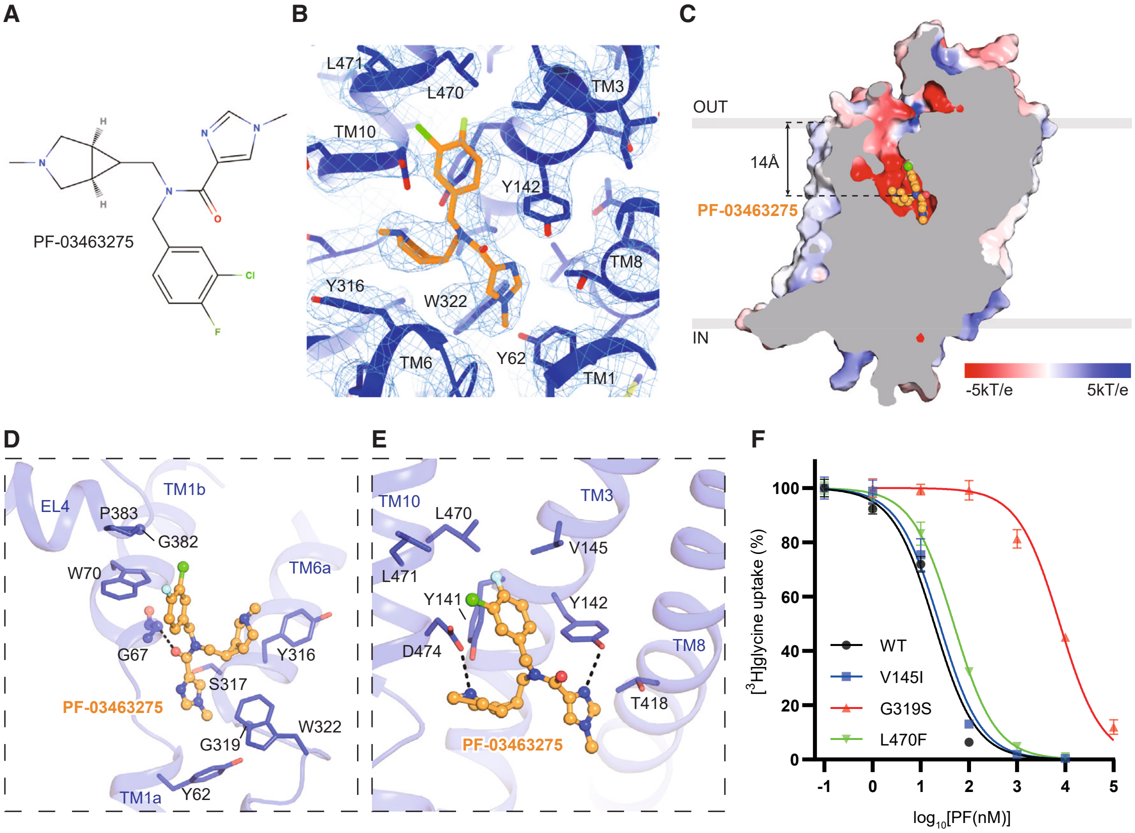

Figure 6. Inhibitory mechanism of PF-03463275

(A) Chemical structure of PF-03463275.

(B) Cryo-EM density (cyan mesh) and model of SSR504734 (orange sticks) binding pocket.

(C) Sagittal slice through an electrostatic surface potential of GlyT1^{PF}. The vertical distance from PF-03463275 (orange sphere) to cytoplasmic membrane plane is labeled.

(D and E) Interaction of PF-03463275 in binding pocket. The key residues for interaction are showed as sticks. The potential hydrogen bonds are represented as dashed lines.

(F) Effect of mutating residues on inhibition potency of PF-03463275. Specified concentrations of PF-03463275 for WT GlyT1, V145I, and L470F are in the range of 0.1 nM to 10 μM, whereas for G319S is in the range of 1 nM to 100 μM. Each point represents mean ± SEM (error bars), n = 3. The [^{3}H]glycine uptake has been normalized to cells without inhibitor treatment. WT and mutants are represented by specific symbols and lines defined in the legend.

See also Figure S5.

that these two LeuT-like transporters undergo comparable conformational transitions during substrate translocation. Previous research have shown that SERT possesses an allosteric serotonin binding site within its extracellular vestibule, which is crucial for regulating its activity.[44,52] However, this site is not conserved in GlyT1 due to TM helix displacements and residue composition variations (Figures S6G–S6I). In our cryo-EM map, no discernible density representing a glycine molecule was observed at a position similar to that in SERT.

Inhibition of GlyT1 by heteroaryl amide PF-03463275

PF-03463275 is a competitive and selective GlyT1 inhibitor,[53] as initial clinical drug of non-sarcosine-based heteroaryl amide series compound developed by Pfizer,[47] and is undergoing phase II trial (NCT01911676) for schizophrenia or schizoaffective disorder treatment. GlyT1 inhibitors from the heteroaryl amide class share common features, including tertiary amides that contain a 5-membered heteroaromatic system, with the amide nitrogen bearing lipophilic benzylic appendages and either a simple alkyl/cycloalkyl or heterocyclic system. We determined the structure of GlyT1 in complex with PF-03463275 (GlyT1^{PF}). The cryo-EM map of GlyT1^{PF} was resolved at 3.0 Å (Figure S1F), which enabled us to reliably build the model. A cloverleaf-shaped density was observed, potentially representing the PF-03463275 molecule (Figure 6B). PF-03463275 interacts with GlyT1 within a cavity that opens toward the extracellular side (Figure 6C), suggesting that GlyT1^{PF} is in an outward-facing conformational state.

The binding pocket of PF-03463275 is composed of TMs 1, 3, 6, 8, and 10, situated 14 Å distance deep from the extracellular leaf of the membrane plane (Figures 6B and 6C). The orientation of PF-03463275 is approximately perpendicular to the membrane plane, with the 1H-imidazole group making contacts with the bottom of cavity and the 3-chloro-4-fluorophenyl group

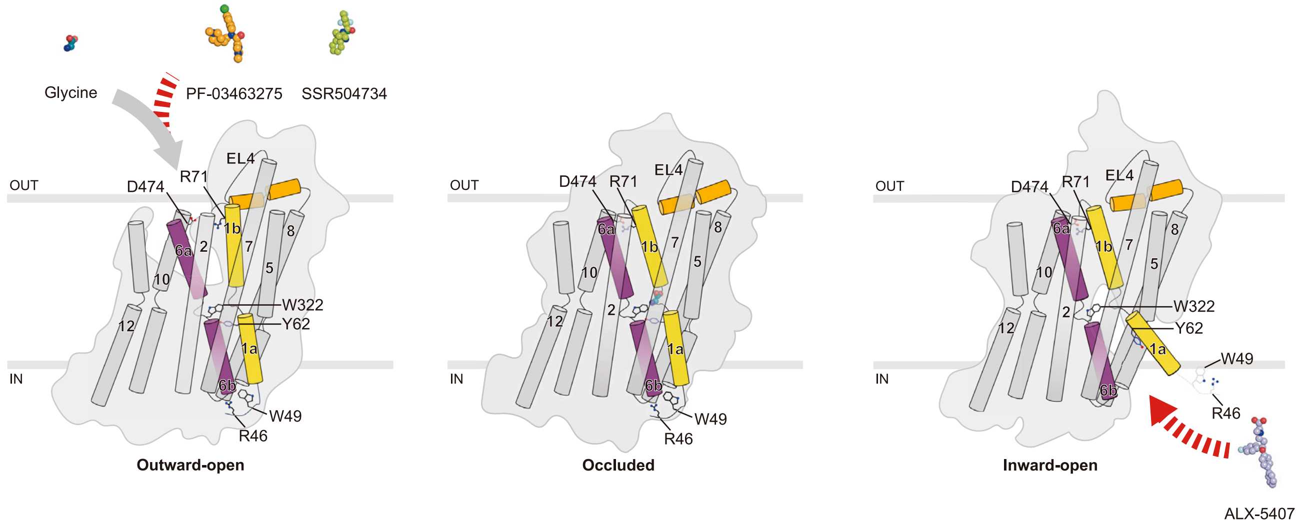

Figure 7. Transport mechanism of and inhibitor action of GlyT1

Schematic depicts conformational differences between outward-open, occluded, and inward-open conformations. TM1, TM6, and EL4 are highlighted in yellow, purple, and orange, respectively. Key residues are depicted in three conformations. SSR504734 (light-green sphere) and PF-03463275 (yellow sphere) access the extracellular cavity and stabilize transporter at its outward-open state. Glycine (green sphere) is determined in occluded state. ALX-5407 (light-purple sphere) stabilizes the transporter in its inward-open state.

pointing toward the extracellular side (Figure 6C). The imidazole group is located in proximity to the unwounded region of TM1 and forms extensive interactions with surround residues, including Y142^{TM3}, W322^{TM6}, and T418^{TM8} (Figures 6D and 6E). In addition, the carboxamide group, positioned on the linker among azabicyclo, imidazole, and 3-chloro-4-fluorophenyl groups, establishes another hydrogen bond with NH2 group of the G67^{TM1}. The azabicyclo group, orienting toward TM10, forms a hydrogen bond with the D474^{TM10} (Figures 6D and 6E). Furthermore, the 3-chloro-4-fluorophenyl group is stabilized by a T-shaped stacking with W70^{TM1}. The residues Y141^{TM3}, V145^{TM3}, and L470^{TM10} engage in hydrophobic interactions with this group as well (Figure 6E). Beyond these direct interactions, the shortest side chains of G67^{TM1}, G319^{TM6}, and G382^{EL4} play a pivotal role in providing sufficient space to accommodate the association of PF-03463275 with GlyT1 (Figure 6D).

Upon superimposition of the GlyT1^{PF} structure onto the GlyT1^{Gly} structure, the binding pocket accommodating the imidazole group largely overlaps with that of the glycine (Figure S5D). The side chains of residues contributing to glycine binding undergo considerable conformational change, a finding that aligns with the competitive inhibition nature of PF-03463275 (Figure S5D). Additionally, we measured the uptake of [^{3}H]glycine by GlyT1 in the absence or presence of varying concentrations of PF-03463275. This analysis revealed the PF-03463275 lowers the apparent affinity of GlyT1 for glycine, whereas the V_{max} remains relatively constant (Figure S5F), further supporting the PF-03463275 functions as a competitive inhibitor. It is also compared with the structure of GlyT1^{SSR}, where the binding pocket partially overlaps but with discernible differences (Figure S5E). The phenyl and piperidin groups of SSR504734 reside in a pocket that is approximately similar to the one housing the azabicyclo and imidazole groups of PF-03463275. The piperidin group of SSR504734 extends toward the TM6, whereas the imidazole group of PF-03463275 reaches the base of the cavity (Figure S5E). Furthermore, PF-03463275 selectively inhibits GlyT1 but has negligible impact on GlyT2.[53] Residues V145^{TM3}, G319^{TM6}, and L470^{TM10} are situated close to the PF-03463275 molecule, and in GlyT2, they are substituted by residues with larger side chains, specifically I290^{T2}, S479^{T2}, and F629^{T2}, respectively (Figure S2). We hypothesize that these substitutions might induce a reduction in the size of the PF-03463275 binding pocket in GlyT2, thus rendering GlyT2 incapable of responding to the inhibitory effect of PF-03463275. To investigate this further, we have designed several mutations, including V145I, G319S, and L470F, to examine their impact on the inhibition of GlyT1 by PF-03463275. It turns out that compared with IC$_{50}$ of approximately 19.0 nM for WT GlyT1, the mutants V145I and L470F slightly increase the IC$_{50}$ of PF-03463275 to approximately 24.4 and 48.0 nM, respectively (Figure 6F). In sharp contrast, the G319S mutation exhibits markedly reduced sensitivity to the PF-03463275, with an IC$_{50}$ value of 7.7 μM, approximately 400 times higher than that of WT GlyT1 (Figure 6F), demonstrating that the residue G319^{TM6} plays a crucial role for PF-03463275 in distinguishing between GlyT1 and GlyT2.

DISCUSSION

The GlyT1 couples the electrochemical gradients of Na$^+$/Cl$^-$ to drive the uphill transport of glycine.[54] In our study, it is captured in three conformational states: inhibitor-bound outward-facing, substrate-bound occluded, and inhibitor-bound inward-facing (Figure 7), which allows us to illustrate the conformational changes occurring during the transport cycle. The TM1 and TM6 play crucial roles in substrate recognition and conformational transition (Figure 7). In the outward-facing state, the TM1, TM3, and TM8 constitute a hydrophilic cavity that allows the substrate to access and binding at the central binding cavity. Once the substrate is bound, the TM1b and TM6a move toward the TM8 and TM10, thereby sealing off the extracellular cavity. The interactions involving residues R71 and D474 may play a crucial role in sealing the extracellular vestibule. The N-terminal loop of GlyT1 is observed to interact with TMD, thereby closing off the intracellular cavity (Figure 7). The residues G67, Y142, Y316, W322, and T418 have been identified as important for recognizing and binding with the glycine. As it transitions to the inward-facing state, the N terminus of GlyT1 dissociates from the TMD. Subsequently, the TM1a helix unwinds further and tilts by 6°, exposing the binding site to the cytosol. In the occluded state, Y62 maintains the integrity of the glycine binding cavity by forming hydrogen bonds with W322. This interaction is disrupted in the inward-facing state, as the Y62 undergoes a significant conformational change.

GlyT1 is a promising therapeutic target for the treatment of behaviors associated with schizophrenia. Numerous inhibitors have been designed and are currently undergoing pre-clinical trials. Our work illustrates how three representative inhibitors bind and inhibit GlyT1. These structures reveal three specific pockets that allow these drugs to exert their inhibitory effects. The classic sarcosine-based inhibitor, ALX-5407, binds non-competitively to the intracellular cavity, preventing the conformational transition from inward-facing to outward-facing states, thus inhibiting GlyT1 activity. The residues G319^{TM6} and L422^{TM8}, replaced by S479 and T582 in GlyT2, are critical for ALX-5407 selectively inhibit GlyT1 over GlyT2. Despite SSR504734 and PF-03463275 both residing at the mouth of the cavity open toward the extracellular side, their binding pockets partially overlap with discernible differences. These two drugs block the vestibule that allows the substrate to enter the central binding cavity and also prevent conformational transition from the outward-facing to occluded state, thus inhibiting GlyT1 activity. Because their binding pockets show significant differences, the residues that determine their selectivity for GlyT1 over GlyT2 are distinct. For SSR504734, the V145^{TM3}/L470^{TM10}/L471^{TM10} residues cluster is critical for its specific inhibition of GlyT1, whereas for PF-03463275, the G319 on the TM6 is vital for discriminating between GlyT1 and GlyT2. Taken together, our study elucidates the molecular basis of substrate-binding, conformational change, as well as the allosteric or competitive, reversible or non-reversible binding modes of anti-schizophrenia drugs, and their selectivity, providing a platform for the rational design of potent, selective, and reversible drugs targeting different conformations, thereby offering potential therapeutic interventions for schizophrenia.

Limitations of the study

This study offers a structural framework for GlyT1 in complex with various anti-schizophrenia compounds, shedding light on their specific binding sites. Through analysis of these complex structures, we observed residue variations within the inhibitor binding pocket between GlyT1 and GlyT2. These differences are proposed to underlie the structural basis for the specificity of these compounds toward GlyT1. However, substituting these residues with those from GlyT2 does not completely eliminate the sensitivity of GlyT1 to these compounds. We speculate that other structural differences between GlyT1 and GlyT2, such as TM displacement, may also contribute to insensitivity of GlyT2 to these compounds. Consequently, a comprehensive understanding of the selective action of these compounds requires more extensive functional and structural studies.

STAR★METHODS

Detailed methods are provided in the online version of this paper and include the following:

- KEY RESOURCES TABLE
- RESOURCE AVAILABILITY
    - ○ Lead contact
    - ○ Materials availability
    - ○ Data and code availability
- EXPERIMENTAL MODEL AND SUBJECT DETAILS
- METHOD DETAILS
    - ○ Clone, expression and purification of human GlyT1
    - ○ Nanodiscs reconstitution
    - ○ Cryo-EM sample preparation and data collection
    - ○ Cryo-EM data processing
    - ○ Model building
    - ○ Thermofluor stability assay
    - ○ [^{3}H]glycine uptake and kinetic assays
- QUANTIFICATION AND STATISTICAL ANALYSIS

SUPPLEMENTAL INFORMATION

Supplemental information can be found online at https://doi.org/10.1016/j.cell.2024.02.026.

ACKNOWLEDGMENTS

We thank X. Huang, B. Zhu, X. Li, and other staff members at the Center for Biological Imaging (CBI), Core Facilities for Protein Science at the Institute of Biophysics, Chinese Academy of Science (IBP, CAS), as well as B. Xu at Peking University Institute of Advanced Agricultural Sciences for their support in cryo-EM data collection. We thank H. Zhang for the support in radioactive experiments. We thank Yan Wu for his research assistant service. The schematic diagram of the graphical abstract was drawn by Figdraw. This work is funded by the Chinese National Programs for Brain Science and Brain-like Intelligence Technology (grant no. 2022ZD0205800 to Y.Z.), the National Key Research and Development Program of China (grant no. 2021YFA1301501 to Y.Z.), the Chinese Academy of Sciences Strategic Priority Research Program (grant no. XDB37030304 to Y.Z.), and the National Natural Science Foundation of China (grant no. 92157102 to Y.Z.).

AUTHOR CONTRIBUTIONS

Y.Z. conceived and supervised the project. T.H. carried out molecular cloning, and Y.W. made all of the mutation constructs. Y.W. and N.L. expressed, purified the protein, and prepared the sample for cryo-EM study. Y.W., R.L., J.Z., and T.H. carried out cryo-EM data collection. R.L. and T.H. processed the cryo-EM data. Y.W. built and refined the atomic model. Y.W., R.L., Y.G., Q.B., and Y.Z. analyzed the structures and prepared the figures. Y.M. and T.H. performed functional assay. Y.Z. prepared and edited the manuscript with input from all authors.

DECLARATION OF INTERESTS

The authors declare no competing interests.

Received: October 2, 2023
Revised: December 9, 2023
Accepted: February 21, 2024
Published: March 20, 2024

REFERENCES

1. Chalphin, A.V., and Saha, M.S. (2010). The specification of glycinergic neurons and the role of glycinergic transmission in development. Front. Mol. Neurosci. *3*, 11.
2. Aprison, M.H., and Werman, R. (1965). The distribution of glycine in cat spinal cord and roots. Life Sci. *4*, 2075–2083.
3. Harvey, R.J., Depner, U.B., Wässle, H., Ahmadi, S., Heindl, C., Reinold, H., Smart, T.G., Harvey, K., Schütz, B., Abo-Salem, O.M., et al. (2004). GlyR alpha3: an essential target for spinal PGE2-mediated inflammatory pain sensitization. Science *304*, 884–887.
4. Werman, R., Davidoff, R., and Aprison, M. (1968). Inhibitory of glycine on spinal neurons in the cat. J. Neurophysiol. *31*, 81–95.
5. Johnson, J.W., and Ascher, P. (1987). Glycine potentiates the NMDA response in cultured mouse brain neurons. Nature *325*, 529–531.
6. Guastella, J., Brecha, N., Weigmann, C., Lester, H.A., and Davidson, N. (1992). Cloning, expression, and localization of a rat brain high-affinity glycine transporter. Proc. Natl. Acad. Sci. USA *89*, 7189–7193.
7. Liu, Q.R., Nelson, H., Mandiyan, S., López-Corcuera, B., and Nelson, N. (1992). Cloning and expression of a glycine transporter from mouse brain. FEBS Lett. *305*, 110–114.
8. Bröer, S., and Gether, U. (2012). The solute carrier 6 family of transporters. Br. J. Pharmacol. *167*, 256–278.
9. Zafra, F., Aragón, C., Olivares, L., Danbolt, N.C., Giménez, C., and Storm-Mathisen, J. (1995). Glycine transporters are differentially expressed among CNS cells. J. Neurosci. *15*, 3952–3969.
10. Jursky, F., and Nelson, N. (1996). Developmental expression of the glycine transporters GLYT1 and GLYT2 in mouse brain. J. Neurochem. *67*, 336–344.
11. Spike, R.C., Watt, C., Zafra, F., and Todd, A.J. (1997). An ultrastructural study of the glycine transporter GLYT2 and its association with glycine in the superficial laminae of the rat spinal dorsal horn. Neuroscience *77*, 543–551.
12. Zeilhofer, H.U. (2005). The glycinergic control of spinal pain processing. Cell. Mol. Life Sci. *62*, 2027–2035.
13. Zafra, F., Ibáñez, I., and Giménez, C. (2017). Glycinergic transmission: glycine transporter GlyT2 in neuronal pathologies. Neuronal Signal. *1*, NS20160009.
14. Cubelos, B., Giménez, C., and Zafra, F. (2005). Localization of the GLYT1 glycine transporter at glutamatergic synapses in the rat brain. Cereb. Cortex *15*, 448–459.
15. Tsai, G., Ralph-Williams, R.J., Martina, M., Bergeron, R., Berger-Sweeney, J., Dunham, K.S., Jiang, Z., Caine, S.B., and Coyle, J.T. (2004). Gene knockout of glycine transporter 1: characterization of the behavioral phenotype. Proc. Natl. Acad. Sci. USA *101*, 8485–8490.
16. Eulenburg, V., Retiounskaia, M., Papadopoulos, T., Gomeza, J., and Betz, H. (2010). Glial glycine transporter 1 function is essential for early postnatal survival but dispensable in adult mice. Glia *58*, 1066–1073.
17. Saha, S., Chant, D., Welham, J., and McGrath, J. (2005). A systematic review of the prevalence of schizophrenia. PLoS Med. *2*, e141.
18. Olney, J.W., Newcomer, J.W., and Farber, N.B. (1999). NMDA receptor hypofunction model of schizophrenia. J. Psychiatr. Res. *33*, 523–533.
19. Nakazawa, K., and Sapkota, K. (2020). The origin of NMDA receptor hypofunction in schizophrenia. Pharmacol. Ther. *205*, 107426.
20. Coyle, J.T. (2006). Glutamate and schizophrenia: beyond the dopamine hypothesis. Cell. Mol. Neurobiol. *26*, 365–384.
21. Lahti, A.C., Weiler, M.A., Tamara Michaelidis, B.A., Parwani, A., and Tamminga, C.A. (2001). Effects of ketamine in normal and schizophrenic volunteers. Neuropsychopharmacology *25*, 455–467.
22. Balu, D.T., and Coyle, J.T. (2015). The NMDA receptor 'glycine modulatory site' in schizophrenia: d-serine, glycine, and beyond. Curr. Opin. Pharmacol. *20*, 109–115.
23. Balu, D.T., Li, Y., Puhl, M.D., Benneyworth, M.A., Basu, A.C., Takagi, S., Bolshakov, V.Y., and Coyle, J.T. (2013). Multiple risk pathways for schizophrenia converge in serine racemase knockout mice, a mouse model of NMDA receptor hypofunction. Proc. Natl. Acad. Sci. USA *110*, E2400–E2409.
24. Wolkenberg, S.E., and Sur, C. (2010). Recent progress in the discovery of non-sarcosine based GlyT1 inhibitors. Curr. Top. Med. Chem. *10*, 170–186.
25. Smith, K.E., Borden, L.A., Hartig, P.R., Branchek, T., and Weinshank, R.L. (1992). Cloning and expression of a glycine transporter reveal colocalization with NMDA receptors. Neuron *8*, 927–935.
26. López-Corcuera, B., Martínez-Maza, R., Núñez, E., Roux, M., Supplisson, S., and Aragón, C. (1998). Differential properties of two stably expressed brain-specific glycine transporters. J. Neurochem. *71*, 2211–2219.
27. Mezler, M., Hornberger, W., Mueller, R., Schmidt, M., Amberg, W., Braje, W., Ochse, M., Schoemaker, H., and Behl, B. (2008). Inhibitors of GlyT1 affect glycine transport via discrete binding sites. Mol. Pharmacol. *74*, 1705–1715.
28. Depoortère, R., Dargazanli, G., Estenne-Bouhtou, G., Coste, A., Lanneau, C., Desvignes, C., Poncelet, M., Heaulme, M., Santucci, V., Decobert, M., et al. (2005). Neurochemical, electrophysiological and pharmacological profiles of the selective inhibitor of the glycine transporter-1 SSR504734, a potential new type of antipsychotic. Neuropsychopharmacology *30*, 1963–1985.
29. Black, M.D., Varty, G.B., Arad, M., Barak, S., De Levie, A., Boulay, D., Pichat, P., Griebel, G., and Weiner, I. (2009). Procognitive and antipsychotic efficacy of glycine transport 1 inhibitors (GlyT1) in acute and neurodevelopmental models of schizophrenia: latent inhibition studies in the rat. Psychopharmacology *202*, 385–396.
30. D'Souza, D.C., Carson, R.E., Driesen, N., Johannesen, J., Ranganathan, M., Krystal, J.H., Ahn, K.-H., Bielen, K., Carbuto, M., and Deaso, E. (2018). Dose-related target occupancy and effects on circuitry, behavior, and neuroplasticity of the glycine transporter-1 inhibitor PF-03463275 in healthy and schizophrenia subjects. Biol. Psychiatry *84*, 413–421.
31. Mchardy, S., and Lowe, J. (2006). Bicyclic [3.1. 0.] heteroaryl amides as type 1 glycine transport inhibitors. U.S. patent application no. 11/399,071.
32. Shahsavar, A., Stohler, P., Bourenkov, G., Zimmermann, I., Siegrist, M., Guba, W., Pinard, E., Sinning, S., Seeger, M.A., Schneider, T.R., et al. (2021). Structural insights into the inhibition of glycine reuptake. Nature *591*, 677–681.
33. Yamashita, A., Singh, S.K., Kawate, T., Jin, Y., and Gouaux, E. (2005). Crystal structure of a bacterial homologue of Na+/Cl–dependent neurotransmitter transporters. Nature *437*, 215–223.
34. Penmatsa, A., Wang, K.H., and Gouaux, E. (2013). X-ray structure of dopamine transporter elucidates antidepressant mechanism. Nature *503*, 85–90.
35. Wang, K.H., Penmatsa, A., and Gouaux, E. (2015). Neurotransmitter and psychostimulant recognition by the dopamine transporter. Nature *521*, 322–327.
36. Motiwala, Z., Aduri, N.G., Shaye, H., Han, G.W., Lam, J.H., Katritch, V., Cherezov, V., and Gati, C. (2022). Structural basis of GABA reuptake inhibition. Nature *606*, 820–826.
37. Coleman, J.A., Green, E.M., and Gouaux, E. (2016). X-ray structures and mechanism of the human serotonin transporter. Nature *532*, 334–339.
38. Zhu, A., Huang, J., Kong, F., Tan, J., Lei, J., Yuan, Y., and Yan, C. (2023). Molecular basis for substrate recognition and transport of human GABA transporter GAT1. Nat. Struct. Mol. Biol. *30*, 1012–1022.

39. Olivares, L., Aragón, C., Giménez, C., and Zafra, F. (1995). The role of N-glycosylation in the targeting and activity of the GLYT1 glycine transporter. J. Biol. Chem. *270*, 9437–9442.

40. Carland, J.E., Thomas, M., Mostyn, S.N., Subramanian, N., O'Mara, M.L., Ryan, R.M., and Vandenberg, R.J. (2018). Molecular Determinants for Substrate Interactions with the Glycine Transporter GlyT2. ACS Chem. Neurosci. *9*, 603–614.

41. Harvey, R.J., Carta, E., Pearce, B.R., Chung, S.K., Supplisson, S., Rees, M.I., and Harvey, K. (2008). A critical role for glycine transporters in hyperexcitability disorders. Front. Mol. Neurosci. *1*, 1.

42. Rees, M.I., Harvey, K., Pearce, B.R., Chung, S.K., Duguid, I.C., Thomas, P., Beatty, S., Graham, G.E., Armstrong, L., Shiang, R., et al. (2006). Mutations in the gene encoding GlyT2 (SLC6A5) define a presynaptic component of human startle disease. Nat. Genet. *38*, 801–806.

43. Zhang, Y.W., Uchendu, S., Leone, V., Bradshaw, R.T., Sangwa, N., Forrest, L.R., and Rudnick, G. (2021). Chloride-dependent conformational changes in the GlyT1 glycine transporter. Proc. Natl. Acad. Sci. USA *118*.

44. Yang, D., and Gouaux, E. (2021). Illumination of serotonin transporter mechanism and role of the allosteric site. Sci. Adv. *7*, eabl3857.

45. Kantrowitz, J., and Javitt, D.C. (2012). Glutamatergic transmission in schizophrenia: from basic research to clinical practice. Curr. Opin. Psychiatry *25*, 96–102.

46. Liu, Q.R., López-Corcuera, B., Mandiyan, S., Nelson, H., and Nelson, N. (1993). Cloning and expression of a spinal cord- and brain-specific glycine transporter with novel structural features. J. Biol. Chem. *268*, 22802–22808.

47. Cioffi, C.L. (2018). Glycine transporter-1 inhibitors: a patent review (2011–2016). Expert Opin. Ther. Pat. *28*, 197–210.

48. Atkinson, B.N., Bell, S.C., Vivo, M.D., Kowalski, L.R., Lechner, S.M., Ognyanov, V.I., Tham, C.-S., Tsai, C., Jia, J., Ashton, D., and Klitenick, M.A. (2001). ALX 5407: A Potent, Selective Inhibitor of the hGlyT1 Glycine Transporter. Mol. Pharmacol. *60*, 1414–1420.

49. Mallorga, P.J., Williams, J.B., Jacobson, M., Marques, R., Chaudhary, A., Conn, P.J., Pettibone, D.J., and Sur, C. (2003). Pharmacology and expression analysis of glycine transporter GlyT1 with [3H]-(N-[3-(4′-fluorophenyl)-3-(4′ phenylphenoxy) propyl]) sarcosine. Neuropharmacology *45*, 585–593.

50. Vandenberg, R.J., Shaddick, K., and Ju, P. (2007). Molecular basis for substrate discrimination by glycine transporters. J. Biol. Chem. *282*, 14447–14453.

51. Coleman, J.A., Yang, D., Zhao, Z., Wen, P.C., Yoshioka, C., Tajkhorshid, E., and Gouaux, E. (2019). Serotonin transporter-ibogaine complexes illuminate mechanisms of inhibition and transport. Nature *569*, 141–145.

52. Neubauer, H.A., Hansen, C.G., and Wiborg, O. (2006). Dissection of an allosteric mechanism on the serotonin transporter: a cross-species study. Mol. Pharmacol. *69*, 1242–1250.

53. Lowe, J.A., 3rd, Hou, X., Schmidt, C., David Tingley, F., 3rd, McHardy, S., Kalman, M., Deninno, S., Sanner, M., Ward, K., Lebel, L., et al. (2009). The discovery of a structurally novel class of inhibitors of the type 1 glycine transporter. Bioorg. Med. Chem. Lett. *19*, 2974–2976.

54. Roux, M.J., and Supplisson, S. (2000). Neuronal and Glial Glycine Transporters Have Different Stoichiometries. Neuron *25*, 373–383.

55. Zheng, S.Q., Palovcak, E., Armache, J.P., Verba, K.A., Cheng, Y., and Agard, D.A. (2017). MotionCor2: anisotropic correction of beam-induced motion for improved cryo-electron microscopy. Nat. Methods *14*, 331–332.

56. Punjani, A., Rubinstein, J.L., Fleet, D.J., and Brubaker, M.A. (2017). cryoSPARC: algorithms for rapid unsupervised cryo-EM structure determination. Nat. Methods *14*, 290–296.

57. Emsley, P., and Cowtan, K. (2004). Coot: model-building tools for molecular graphics. Acta Crystallogr. D Biol. Crystallogr. *60*, 2126–2132.

58. Pettersen, E.F., Goddard, T.D., Huang, C.C., Couch, G.S., Greenblatt, D.M., Meng, E.C., and Ferrin, T.E. (2004). UCSF Chimera—a visualization system for exploratory research and analysis. J. Comput. Chem. *25*, 1605–1612.

59. Adams, P.D., Afonine, P.V., Bunkóczi, G., Chen, V.B., Davis, I.W., Echols, N., Headd, J.J., Hung, L.-W., Kapral, G.J., Grosse-Kunstleve, R.W., et al. (2010). PHENIX: a comprehensive Python-based system for macromolecular structure solution. Acta Crystallogr. D Biol. Crystallogr. *66*, 213–221.

60. Mastronarde, D.N. (2005). Automated electron microscope tomography using robust prediction of specimen movements. J Struct. Biol. *152*, 36–51.

61. Goddard, T.D., Huang, C.C., Meng, E.C., Pettersen, E.F., Couch, G.S., Morris, J.H., and Ferrin, T.E. (2018). UCSF ChimeraX: Meeting modern challenges in visualization and analysis. Protein Sci *27*, 14–25.

STAR★METHODS

KEY RESOURCES TABLE

REAGENT or RESOURCE	SOURCE	IDENTIFIER
Bacterial and virus strains		
DH5α	Yeasen Biotech	11802ES80
DH10Bac	Invitrogen	10359-016
Chemicals, peptides, and recombinant proteins		
Recombinantly expressed GlyT1	This study	N/A
Recombinantly expressed MSP1D1E3	This study	N/A
Recombinantly expressed HRV3C protease	This study	N/A
n-Dodecyl-b-D-Maltopyranoside (DDM)	Shanghai Yuanye Bio-Technology	S11168
Lauryl maltose neopentyl glycol (LMNG)	Anatrace	NG310
Glyco-diosgenin (GDN)	Anatrace	GDN101
Fluorinated octyl maltoside (FOM)	Anatrace	O310F
Digitonin	Biosynth	D-3200
Triton X-100	Sigma Aldrich	X100
Cholesteryl hemisuccinate tris salt (CHS)	Anatrace	CH210
N-[4-7- (diethylamino-4-methyl-3-coumarinyl) phenyl] maleimide (CPM)	Invitrogen	D346
Aprotinin	MedChemExpress	HY-P0017
Leupeptin hemisulfate	MedChemExpress	HY-18234A
Pepstatin A	MedChemExpress	HY-P0018
4-(2-hydroxyethyl)-1-piperazineethanesulfonic acid (HEPES)	VWR Chemicals	0511
Tris	Sigma-Aldrich	11814273001
D-Desthiobiotin	Leyan	1169249
Imidazole	Sigma-Aldrich	I5513
Sodium butyrate	Sigma-Aldrich	303410
Sodium chloride	Sigma-Aldrich	S5886
Potassium chloride	Beijing Yili Fine Chemicals	6-1
Magnesium chloride	Beijing Yili Fine Chemicals	7-22
Calcium chloride	Beijing Yili Fine Chemicals	7-2
Magnesium sulfate	Beijing Yili Fine Chemicals	7-25
Glycine	VWR Chemicals	0167
Glucose	Tianjin ZhiYuan Reagent	20220601820
Brain polar lipid extract	Avanti	141101C
Bio-Beads SM2 adsorbent	Bio-Rad	1523920
PF-03463275	MedChemExpress	HY-10716A
SSR504734	Leyan	615571-23-8
ALX-5407 hydrochloride	Tocris Bioscience	1757
Dimethyl sulfoxide (DMSO)	Amresco	0231
[^{3}H]glycine (GLYCINE, [2-^{3}H]-)	PerkinElmer	NET004
Optiphase supermix	PerkinElmer	1200-439
OPM-293 CD05 Medium	OPM	81075-001
IB905 Medium	Yishengke Biotechnology	L11001
Critical commercial assays		
FastPure Plasmid Mini Kit	Vazyme Biotech	DC201-01
BCA Protein Assay Kit	Beyotime	P0010

(*Continued on next page*)

Continued

REAGENT or RESOURCE	SOURCE	IDENTIFIER
Deposited data		
GlyT1^{Gly}, atomic model	Protein Data Bank	8WFI
GlyT1^{Gly}, EM density map	Electron Microscopy Data Bank	EMD-37492
GlyT1^{ALX}, atomic model	Protein Data Bank	8WFJ
GlyT1^{ALX}, EM density map	Electron Microscopy Data Bank	EMD-37493
GlyT1^{SSR}, atomic model	Protein Data Bank	8WFK
GlyT1^{SSR}, EM density map	Electron Microscopy Data Bank	EMD-37494
GlyT1^{PF}, atomic model	Protein Data Bank	8WFL
GlyT1^{PF}, EM density map	Electron Microscopy Data Bank	EMD-37495
Experimental models: Cell lines		
HEK293F	Gibco	R79007
Sf9	Gibco	11496015
Oligonucleotides		
GlyT1-F: GGAGCTGGCAGAGGTGTGAAT	Tsingke Biotechnology	N/A
GlyT1-R: TCCCCTGGCAGCTGTGCTCATAT	Tsingke Biotechnology	N/A
GlyT1-R46E-F: ACCTCAAAGAGGGCAACTGGGGCAAC	Tsingke Biotechnology	N/A
GlyT1-R46E-R: CAGTTGCCCTCTTTGAGGTTCTGGTC	Tsingke Biotechnology	N/A
GlyT1-W49Q-F: GGGGCAACCAGGGCAACCAGATCGAGT	Tsingke Biotechnology	N/A
GlyT1-W49Q-R: GTTGCCCTGGTTGCCCCGTTTGAGGT	Tsingke Biotechnology	N/A
GlyT1-Y62A-F: GCGTGGGCGCAGCCGTGGGCCTGGGCA	Tsingke Biotechnology	N/A
GlyT1-Y62A-R: CCCACGGCTGCGCCCACGCTCGTCAGT	Tsingke Biotechnology	N/A
GlyT1-G65A-F: TGCCGTGGCCCTGGGCAATGTCTG	Tsingke Biotechnology	N/A
GlyT1-G65A-R: TGCCCAGGGCCACGGCATAGCCCAC	Tsingke Biotechnology	N/A
GlyT1-G67S-F: GTGGGCCTGAGTAATGTCTGGCGCTTCCCA	Tsingke Biotechnology	N/A
GlyT1-G67S-R: CAGACATTACTCAGGCCCACGGCATA	Tsingke Biotechnology	N/A
GlyT1-N68A-F: GCCTGGGCGCTGTCTGGCGCTTCCCA	Tsingke Biotechnology	N/A
GlyT1-N68A-R: GCCAGACAGCGCCCAGGCCCACGGCA	Tsingke Biotechnology	N/A
GlyT1-R71A-F: CAATGTCTGGGCATTCCCATACCTCTGCT	Tsingke Biotechnology	N/A
GlyT1-R71A-R: TATGGGAATGCCCAGACATTGCCCAG	Tsingke Biotechnology	N/A
GlyT1-R71D-F: TGTCTGGGACTTCCCATACCTCTGCT	Tsingke Biotechnology	N/A
GlyT1-R71D-R: TATGGGAAGTCCCAGACATTGCCCAG	Tsingke Biotechnology	N/A
GlyT1-R71K-F: ATGTCTGGAAGTTCCCATACCTCTGCT	Tsingke Biotechnology	N/A
GlyT1-R71K-R: TATGGGAACTTCCAGACATTGCCCAG	Tsingke Biotechnology	N/A
GlyT1-Y142A-F: GCATCTACGCAAATGTGGTCATCTGCA	Tsingke Biotechnology	N/A
GlyT1-Y142A-R: GACCACATTTGCGTAGATGCCGATGTA	Tsingke Biotechnology	N/A
GlyT1-V145I-F: ACAATGTGATAATCTGCATCGCCTTC	Tsingke Biotechnology	N/A
GlyT1-V145I-R: GATGCAGATTATCACATTGTAGTAGATG	Tsingke Biotechnology	N/A
GlyT1-Y316A-F: CAGATCTTCGCCTCACTGGGCTGCGCG	Tsingke Biotechnology	N/A
GlyT1-Y316A-R: CCAGTGAGGCGAAGATCTGGGAGGCAG	Tsingke Biotechnology	N/A
GlyT1-S317A-F: TCTTCTACGCACTGGGCTGCGCGTG	Tsingke Biotechnology	N/A
GlyT1-S317A-R: AGCCCAGTGCGTAGAAGATCTGGGAG	Tsingke Biotechnology	N/A
GlyT1-G319L-F: TCACTGCTCTGCGCGTGGGGAGGCCT	Tsingke Biotechnology	N/A
GlyT1-G319L-R: CACGCGCAGAGCAGTGAGTAGAAG	Tsingke Biotechnology	N/A
GlyT1-G319Q-F: CTCACTGCAGTGCGCGTGGGGAGGCCT	Tsingke Biotechnology	N/A
GlyT1-G319Q-R: CACGCGCACTGCAGTGAGTAGAAGATC	Tsingke Biotechnology	N/A

(*Continued on next page*)

Continued

REAGENT or RESOURCE	SOURCE	IDENTIFIER
GlyT1-G319S-F: CTCACTGAGTTGCGCGTGGGGAGGC	Tsingke Biotechnology	N/A
GlyT1-G319S-R: CACGCGCAACTCAGTGAGTAGAAGATC	Tsingke Biotechnology	N/A
GlyT1-W322A-F: GCTGCGCGGCAGGAGGCCTCATCACCA	Tsingke Biotechnology	N/A
GlyT1-W322A-R: GAGGCCTCCTGCCGCGCAGCCCAGTGAG	Tsingke Biotechnology	N/A
GlyT1-W322F-F: GCTGCGCGTTCGGAGGCCTCATCAC	Tsingke Biotechnology	N/A
GlyT1-W322F-R: AGGCCTCCGAACGCGCAGCCCAGTGAG	Tsingke Biotechnology	N/A
GlyT1-W322L-F: GCTGCGCGCTGGGAGGCCTCATCACCAT	Tsingke Biotechnology	N/A
GlyT1-W322L-R: GAGGCCTCCCAGCGCGCAGCCCAGTGAG	Tsingke Biotechnology	N/A
GlyT1-N349A-F: GCATCACCGCATGTGCCACCAGCGTC	Tsingke Biotechnology	N/A
GlyT1-N349A-R: GTGGCACATGCGGTGATGCTGATGATG	Tsingke Biotechnology	N/A
GlyT1-T418A-F: GGCTGGGCGCTCAGTTCTGCCTCCT	Tsingke Biotechnology	N/A
GlyT1-T418A-R: CAGAACTGAGCGCCCAGCCCCAGCAG	Tsingke Biotechnology	N/A
GlyT1-T418Q-F: GGCTGGGCCAACAGTTCTGCCTCCTG	Tsingke Biotechnology	N/A
GlyT1-T418Q-R: CAGAACTGTTGGCCCAGCCCCAGCAG	Tsingke Biotechnology	N/A
GlyT1-L422T-F: CAGTTCTGCACTCTGGAGACGCTGGTC	Tsingke Biotechnology	N/A
GlyT1-L422T-R: TCTCCAGAGTGCAGAACTGAGTGCCCA	Tsingke Biotechnology	N/A
GlyT1-L470F-F: TCTATTGGTTCCTGCTGATGGACAACT	Tsingke Biotechnology	N/A
GlyT1-L470F-R: TCAGCAGGAACCAATAGATGCCTGCCT	Tsingke Biotechnology	N/A
GlyT1-L471Q-F: TTGGCTGCAGCTGATGGACAACTATG	Tsingke Biotechnology	N/A
GlyT1-L471Q-R: CCATCAGCTGCAGCCAATAGATGCCT	Tsingke Biotechnology	N/A
GlyT1-L470F-L471Q-F: TTGGTTCCAGCTGATGGACAACTATG	Tsingke Biotechnology	N/A
GlyT1-L470F-L471Q-R: CATCAGCTGGAACCAATAGATGCCT	Tsingke Biotechnology	N/A
GlyT1-D474A-F: TGCTGATGGCAAACTATGCGGCCAGCT	Tsingke Biotechnology	N/A
GlyT1-D474A-R: GCATAGTTTGCCATCAGCAGCAGCCAATAG	Tsingke Biotechnology	N/A
GlyT1-D474E-F: CTGATGGAGAACTATGCGGCCAGCT	Tsingke Biotechnology	N/A
GlyT1-D474E-R: GCATAGTTCTCCATCAGCAGCAGC	Tsingke Biotechnology	N/A
GlyT1-D474R-F: GCTGATGAGAAACTATGCGGCCAGCT	Tsingke Biotechnology	N/A
GlyT1-D474R-R: GCATAGTTTCTCATCAGCAGCAGCCAATAG	Tsingke Biotechnology	N/A
Recombinant DNA		
Full-length human GlyT1b	This study	UniProt ID: P48067-3
Software and algorithms		
SerialEM	Mastronarde[60]	https://bio3d.colorado.edu/SerialEM/
EPU	Thermo Fisher Scientific	http://www.thermofisher.com/
MotionCor2	Zheng et al.[55]	https://emcore.ucsf.edu/ucsf-software/
cryoSPARC	Punjani et al. [56]	https://cryosparc.com/
Coot	Emsley and Cowtan[57]	https://www2.mrc-lmb.cam.ac.uk/personal/pemsley/coot/
Open-Source PyMOL	Schrödinger, Inc.	https://pymol.org/
UCSF Chimera	Pettersen et al.[58]	https://www.cgl.ucsf.edu/chimera/
UCSF ChimeraX	Goddard et al.[61]	https://www.rbvi.ucsf.edu/chimerax/
Phenix	Adams et al. [59]	https://phenix-online.org
Prism 9	GraphPad	https://www.graphpad.com/

RESOURCE AVAILABILITY

Lead contact

Further information and requests for resources and reagents will be directed and be fulfilled by Yan Zhao (zhaoy@ibp.ac.cn), the lead contact.

Materials availability

Plasmids generated in this study are freely available on request.

Data and code availability

- Atomic model of GlyT1^{Gly}, GlyT1^{ALX}, GlyT1^{SSR} and GlyT1^{PF} have been deposited in the PDB and are publicly available under the accession codes 8WFI, 8WFJ, 8WFK and 8WFL. The cryo-EM density of GlyT1^{Gly}, GlyT1^{ALX}, GlyT1^{SSR} and GlyT1^{PF} are available in the Electron Microscopy Data Bank under the accession codes EMD-37492, EMD-37493, EMD-37494 and EMD-37495, respectively. All other microscopy data reported will be shared by the lead contact upon request.
- This paper does not report original code.
- Any additional information required to reanalyze the data reported in this paper is available from the lead contact upon request.

EXPERIMENTAL MODEL AND SUBJECT DETAILS

DH5α (Yeasen Biotech) and DH10Bac (Invitrogen) were cultured in lysogeny broth (LB) at 37°C and 5% CO_2 to amplify plasmids.

HEK293F cells (Gibco, R79007) were cultured in OPM-293 CD05 Medium (OPM, 81075-001) at 37°C and 5% CO_2.

Sf9 cells (Gibco, 11496015) were cultured in IB905 Medium (Yishengke Biotechnology, L11001) at 27°C and 5% CO_2.

METHOD DETAILS

Clone, expression and purification of human GlyT1

The DNA coding full-length wild type human GlyT1b (*SLC6A9*, Uniprot: P48067-3) was cloned into the pEG BacMam vector with a C-terminal superfolder GFP (sfGFP) followed by a Twin-Strep affinity tag. A PreScission protease site (LEVLFQ/GP) is present between GlyT1b and C-terminal GFP. The Bac-to-Bac system was used to produce recombinant baculovirus in sf9 cells. The HEK293F cells at density of ~2 x 10^6 cells per mL were infected with 2% (v/v) P2 recombinant baculovirus and subsequently cultured at 37°C with 5% CO2. After 12 h, 10 mM sodium butyrate was added to the medium for enhancing protein expression. The cells were harvested 60 h after infection.

The cell pellets were resuspended on ice in buffer A containing 20 mM HEPES pH 7.5, 150 mM NaCl, 2 μg/mL aprotinin, 1.4 μg/mL leupeptin, 0.5 μg/mL pepstatin A. Cell membranes were enriched by centrifugation at 37,000 rpm for 30 min at 4°C. The collected membrane pellets were solubilized with 1% (w/v) n-dodecyl-β-D-maltoside (DDM) and 0.15% (w/v) cholesteryl hemisuccinate (CHS) (Anatrace, USA) in buffer A for 2 h at 4°C. Insoluble material was removed by centrifugation at 38,000 rpm for 30 min. The supernatant was passed through the 0.22 μm filter and then applied to a streptavidin resin for protein affinity purification. Following loading of the sample, the resin was washed with buffer B containing 20 mM HEPES pH 7.5, 150 mM NaCl, 0.025% DDM, and additional 1 μM PF-03463275 or 1 μM SSR504734 or 1 μM ALX-5407 or 20 mM Glycine respectively. The GlyT1 protein was then eluted with buffer C containing 20 mM HEPES pH 7.5, 150 mM NaCl, 0.1% digitonin, and additionally containing 5 mM desthiobiotin. The elution was concentrated to a final volume of 1 mL with 50-kDa Millipore Tube (Merck Millipore, Germany) and further purified through size exclusion chromatography (SEC) using a Superose 6 Increase 10/300 GL column (GE Healthcare, USA) equilibrated with buffer D containing 20 mM HEPES pH 7.5, 150 mM NaCl, 0.1% digitonin, and. The peak fractions were collected and concentrated to ~1 mg/mL for the following nanodisc reconstitution. To determine glycine-bound and inhibitor-bound structures, we supplemented 20 mM glycine or 1μM inhibitors throughout the purification process.

Nanodiscs reconstitution

The nanodisc reconstitution was carried out with membrane scaffold protein MSP1D1E3. MSP1D1E3 was purified through a metal chelate affinity column (Ni-NTA) and extensive dialysis against in TBS buffer (20 mM Tris pH 8.0, 150 mM KCl). To incorporate the transporter in lipid nanodisc, brain polar lipid (BPL, Avanti) dissolved in chloroform was dried down using vacuum dryer and resuspended in HBS buffer (20 mM HEPES pH 7.5, 150 mM NaCl) to a final concentration 30mg/mL, eventually was supplemented with 2% (w/v) digitonin and incubated at 4°C for 30min before used. GlyT1 protein was mixed with MSP1D1E3 and brain polar lipid (BPL) in a final molar ratio (GlyT1: MSP1D1E3: BPL) of 1:5:200 and gently tumbled at 4°C for 1h. To remove detergent, Bio-Beads (SM2, Bio-Rad) were then added to the mixture in final concentration 400 mg/mL and incubated at 4 °C for 1 h and then replaced with fresh Bio-Beads twice. After the final replacement of Bio-Beads, the mixture was incubated overnight by gentle agitation at 4 °C. The Biobeads were separated through centrifugation and the supernatant was load into streptavidin resin and washed by buffer E containing 20 mM HEPES pH 7.5, 150 mM NaCl, to remove empty nanodiscs. The reconstituted GlyT1 protein was eluted with buffer E additionally containing 4 mM desthiobiotin. The elution was digested with HRV3C protease at 4°C for 1h to remove the sfGFP tag of GlyT1. After digestion, the final concentration of 15 mM imidazole was added to the protein sample and then applied to the Ni-NTA resin and washed by buffer E supplemented with 20 mM imidazole to remove HRV3C protease. The flow through sample and washed sample were collected then mixed and concentrated to a final volume of 1 mL and further loaded onto Superose 6 Increase 10/300 GL column equilibrated with buffer E. The peak fractions around ~15.5 mL were collected and concentrated to 5~6 mg/mL for cryo-EM grids preparation.

Cryo-EM sample preparation and data collection

A final concentration of 1 mM ALX-5407, 200 μM SSR504734 and 100 μM PF-03463275 (MedChemExpress, MCE) were added to the cryo-EM sample for GlyT1^{ALX}, GlyT1^{SSR} and GlyT1^{PF}, respectively, and incubated 40 min on ice before application in grids. Specially 60 μM Fluorinated Octyl Maltoside (FOM, Anatrace, USA) was added to the the cryo-EM sample for GlyT1^{SSR} with SSR504734 at the same time. Quantifoil 1.2/1.3 Cu 300 mesh grids was glow-discharged for 60 s under H_2-O_2 condition with a Solarus plasma cleaner (Gatan, USA) before using. The grids were applied with a 3-μL droplet of protein sample at 4°C and 100% humidity, and then snap-frozen in liquid ethane cooled by liquid nitrogen using a Vitrobot Mark IV (Thermo Fisher Scientific, USA). The grids sample was stored in liquid nitrogen before being checked on the electron microscopy instrument.

For GlyT1^{ALX} and GlyT1^{PF}, cryo-EM data were collected on a 300-kV Titan Krios (Thermo Fisher Scientific, UAS) equipped with a K2 Summit direct electron detector (Gatan, USA) and a GIF-Quantum LS energy filter. The energy filter slit width was set to 20 eV. Movie stacks were acquired using SerialEM at a calibrated magnification of 165,000 x in the super-resolution mode, with defocus values ranging from −1.2 to −2.2 μm. The pixel size on motion-corrected micrographs was 0.82 Å. Each movie stack was dose-fractioned in 32 frames, yielding a total accumulated dose of 60 $e^-/Å^2$ The dose rate was set to 9.6 e^-/pixel/s.

For GlyT1^{Gly} and GlyT1^{SSR}, cryo-EM data were collected on a 300-kV Titan Krios G4 (Thermo Fisher Scientific, UAS) equipped with a K3 Summit direct electron detector (Gatan, USA) and a GIF-Quantum LS energy filter. The energy filter slit width was set to 20 eV. Movie stacks were acquired using EPU software at a calibrated magnification of 105,000 x in the super-resolution mode, with defocus values ranging from −1.0 to −2.0 μm. The pixel size on motion-corrected micrographs was 0.85 Å. Each movie stack was dose-fractioned in 32 frames, yielding a total accumulated dose of 60 $e^-/Å^2$ The dose rate was set to 15 e^-/pixel/s.

Cryo-EM data processing

For GlyT1^{Gly}, GlyT1^{ALX}, GlyT1^{SSR} and GlyT1^{PF} dataset, 3196, 2955, 2280, and 1762 super-resolution movie stacks were aligned, summed, dose-weighted and bin by 2 using the program MotionCor2,[55] and then imported into cryoSPARC.[56] The defocus value of each image was determined by patch CTF (contrast transfer function) estimation. Micrographs showing contamination or a bad CTF estimation were excluded during manual curation. The processing of GlyT1^{Gly}, GlyT1^{ALX}, GlyT1^{SSR} and GlyT1^{PF} adopted a similar scheme of classification and refinement, therefore the detailed procedures were introduced with GlyT1^{PF} dataset processing as example (Figure S1F). The processing of GlyT1^{Gly}, GlyT1^{ALX}, and GlyT1^{SSR} datasets were illustrated in flowchart (Figures S1G–S1I).

For the GlyT1^{PF} dataset initial round, 770k particles were autopicked by blob-picker from 700 micrographs. Particle sets were extracted using a box size of 256 pixels and a pixel size of 0.82 Å, followed by several rounds of 2D classification until distinguishable transmembrane domain (TMD) density was achieved. An initial 3D model was generated through ab-initio reconstruction of these 2D classes. Two rounds of heterogenous refinement were carried out using the initial 3D model and five biased maps to exclude artifacts and undesirable particles. Particles from good classes were merged and duplicates were removed, yielding 115k good particles. Subsequently, non-uniform refinement was performed using these particles and generating a 4.6 Å map with clear TM helices, which served as "seed" for the following process. To further improve the resolution, 1,809k particles were picked using the template picker for seed-facilitated 3D classification. Iterative rounds heterogenous refinement for multi-reference 3D classification were carried out on these particles, yielding 161k high-quality particles. Following 3D classification without alignment (3 classes), local refinement was performed using a manually created mask, leading to a reconstruction of the GlyT1^{PF} dataset at an average resolution of 3.0 Å. For GlyT1^{Gly}, GlyT1^{ALX}, and GlyT1^{SSR} datasets, similar procedures were applied and 1,041,324, 154,181 and 51,093 particles gave rise to 2.6 Å, 3.3 Å and 3.2 Å average resolution reconstruction map respectively.

The overall resolution of the final map of GlyT1^{Gly}, GlyT1^{ALX}, GlyT1^{SSR} and GlyT1^{PF} was determined by the gold-standard Fourier shell correlation (FSC), and the local resolution estimation was performed to determine the local resolution of the final map in the cryoSPARC. The angular distribution of the particles selected for the final refinement is reasonable.

Model building

The initial model was built manually in COOT[57] according to the electron density of GlyT1^{PF}. Then, the model was manually adjusted in COOT iteratively, including the refinement of mainchain and sidechains of residues. Structure refinement was performed using phenix.real_space_refine application in PHENIX[59] in real space with secondary structure and Ramachandran restraints. For the ligand building of GlyT1^{PF}, the two-dimension (2D) structure of PF-03463275 were downloaded from PubChem in the SDF format, followed by the generation of 3D models and refinement restraints in phenix.ligand_eLBOW.[59] These ligands molecules were docked into the EM map and the overlay was optimized according to the corresponding density. To build the SSR504734-bound structures, the above determined structure GlyT1^{PF} was fitted to the density maps using UCSF chimera. After rigid-body fitting of the GlyT1^{PF} model, PF-03463275 molecule was replaced with SSR504734 produced by similar procedure of PF-03463275, and the models were then real-space refined in Coot and Phenix.[59] The GlyT1^{Gly} structure was achieved by fitting the GlyT1^{PF} to its corresponding map using UCSF Chimera. Coot was then used to manually adjust the GlyT1^{Gly} structure, followed by Phenix refinement. For GlyT1^{Gly}, four sphere density near A63, Y316, G319, W322 and near Q313, S317 was judged to be glycine, putative sodium ions and putative chlorine ion, respectively. The structure of GlyT1^{ALX} were built by similar procedures. The final model of GlyT1^{PF} lacks residues 1-43 in N-terminus, residues 182-201 in EL2, and residues 615-652 in C-terminus.

All figures were prepared with software Pymol or UCSF Chimera.[58]

Thermofluor stability assay

Thermofluor analysis was performed with a quantitative PCR instrument (Rotor-Gene 6600, Corbett Research, Australia). Thiol-specific fluorochrome N-[4-7- (diethylamino-4-methyl-3-coumarinyl) phenyl] maleimide (CPM, invitrogen, US) was used as the fluorescence probe. CPM fluorescence signal was measured with a 387-nm excitation and a 463-nm emission. The purified protein of GlyT1 (2 μg/μL) was added into assay buffer at 0.2 μg/μL final concentration with different detergents (20 mM HEPES, pH 7.5, 150 mM NaCl, 0.025% DDM or 0.01% LMNG or 0.01% GDN or 0.1% digitonin). The CPM stock (4 mg/mL in DMSO) was diluted 16-fold in sterile water and then added 1 μL to the system in the dark. The total reaction volume was 25 μL. The quantitative PCR instrument was programed to increase temperature by 1°C in 1 min from 25°C to 95°C. Data analyses were performed using the program Graphpad Prism.

[^{3}H]glycine uptake and kinetic assays

HEK293-F cells were infected with various GlyT1 construction viruses at a cell density of 2.5 x 10^6 and then cultured at 37°C with 5% CO_2 for ~15 hours before uptake and kinetic assays. Fifteen hours post-transfection, 2 x 10^6 cells were used for each reaction. The cells were washed once with uptake buffer (10 mM HEPES-Tris, pH 7.4, 150 mM NaCl, 1 mM $CaCl_2$, 5 mM KCl, 1 mM $MgSO_4$, and 10 mM glucose). The [^{3}H]glycine uptake was initiated by adding a 25 μM mixture of [^{3}H]glycine and unlabeled glycine at a ratio of 1:2500 and the uptake was carried out at room temperature. The uptake duration was set to 1 minute, based on preliminary experiments to ensure the uptake occurs within linear range. The reaction was stopped by adding cold (4°C) uptake buffer, followed by centrifugation and rapid removal of the supernatant. The cells were then washed twice with cold uptake buffer to remove any free isotope. In the inhibition assays, cells were preincubated with varying concentrations of inhibitors PF-03463275 and SSR504734 for 10 minutes, and ALX-5407 for 15 minutes at room temperature prior to initiating the uptake reaction. The cells were subsequently incubated with 25 μM of [^{3}H]glycine for 1 minute and the uptake assay was carried out as described above. For kinetic uptake studies, the substrate glycine was prepared by mixing [^{3}H]glycine and unlabeled glycine in a 1:8000 molar ratio. To determinate the Km and maximal velocity V_{max} of WT GlyT1 and its mutants, uptake was initiated by addition of 37.5–900 μM [^{3}H]glycine in a final volume of 150 μL of uptake buffer. To assess competitive inhibition effect, inhibitors PF-03463275 (100 or 200 nM) or SSR504734 (300 or 600 nM) were supplemented into the uptake buffer without preincubation. After 1 minute of incubation with [^{3}H]glycine at room temperature, the cells were washed twice with 800 μL of ice-cold uptake buffer to terminate the reaction. The cells were then lysed in 200 μL uptake buffer supplemented with 1% Triton X-100 at room temperature for 5 minutes. The lysate was subsequently transferred to a tube containing 2 mL scintillating agent (Optiphase Supermix, PerkinElmer). The expression levels of various constructs were determined by fluorescent-based high-performance liquid chromatography. Radioactivity was measured using a Hidex 300 SL liquid scintillation counter (Hidex, Finland) for 20 seconds per tube. Data were obtained from three biologically independent experiments and analyzed using nonlinear regression using the equation: $Y=100/(1+10^{(X-LogIC50)})$ in GraphPad Prism9. Kinetic parameters (K_m and V_{max}) were calculated using the equation: $Y=V_{max} \times X/(K_m + X)$ in GraphPad Prism9 and the curve was fitted using the mean of plots from three independent experiments.

QUANTIFICATION AND STATISTICAL ANALYSIS

All functional experiments data were obtained from three biologically independent experiments unless otherwise specified and were presented as mean ± SEM in graphs. IC_{50} and kinetic parameters were calculated using GraphPad 9.0. Operations of normalization were performed as indicated in figure legend. P values were calculated by unpaired t-tests or one-way ANOVA followed by Dunnett's test and $P < 0.05$ represent significant difference.

Supplemental figures

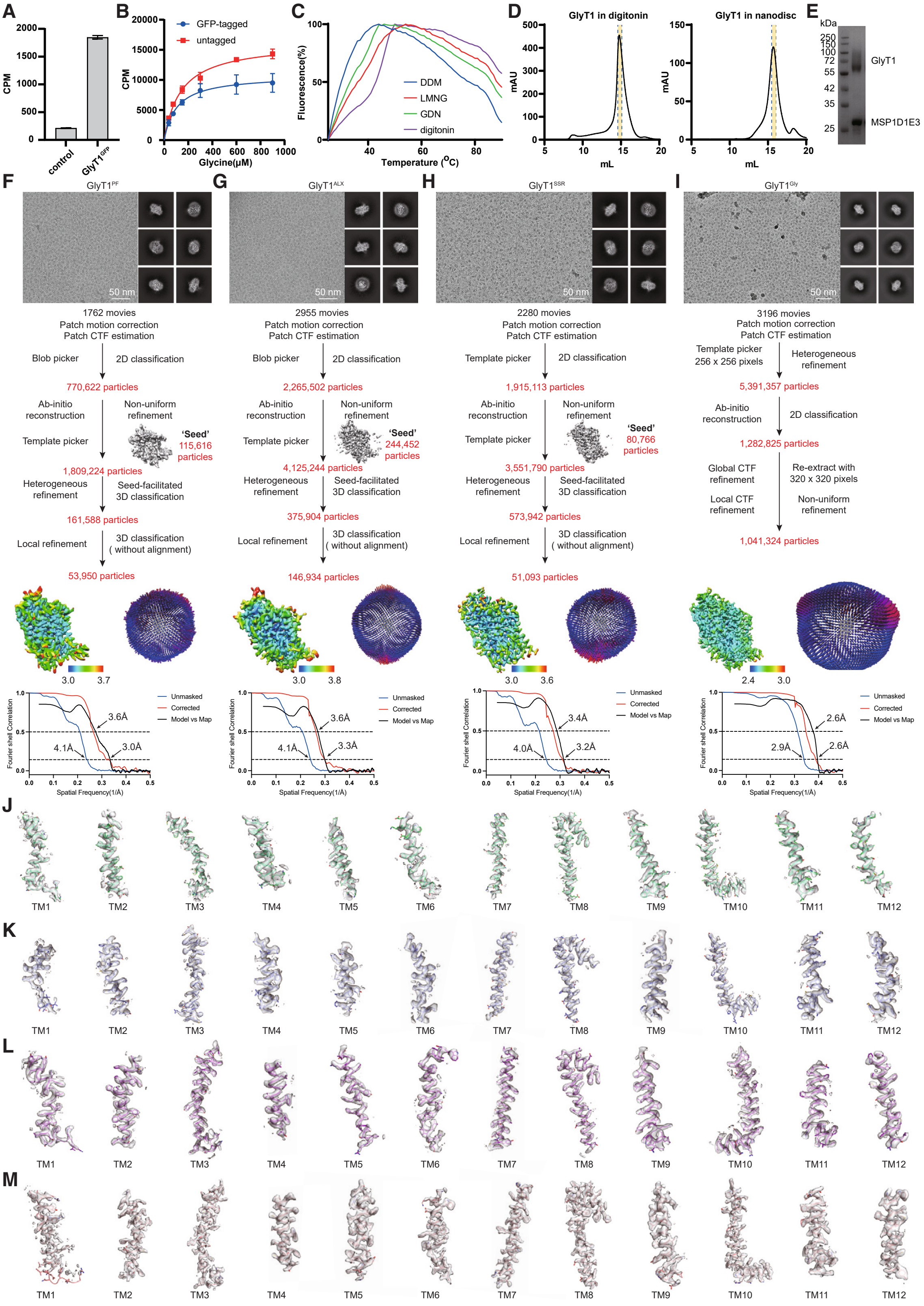

(legend on next page)

Figure S1. Functional characterization, purification, and cryo-EM data processing of GlyT1, related to STAR Methods

(A) The transport activity of GFP-tagged wild-type GlyT1, quantified by [^{3}H]glycine uptake assay and normalized by BCA (bicinchoninic acid) protein assay. Negative control is untransfected HEK293 cells. Data represent mean ± SEM for three independent experiments.

(B) The transport activity of GFP-tagged and untagged wild-type GlyT1 was quantified by [^{3}H]glycine uptake assay, and fitted in Michaelis-Menten equation. The K_m of GFP-tagged ($n = 6$) and untagged ($n = 3$) GlyT1 are 104.9 and 140.9 μM, respectively; p value > 0.05 with unpaired t test, no statistically significant difference. The background activity of negative control (untransfected HEK293 cells) is subtracted from final data. Data represent mean ± SEM (error bars).

(C) Thermofluor assay of GlyT1 in the presence of various detergents shows different thermal stability of GlyT1.

(D) Representative profile of the GlyT1 proteins in digitonin or reconstituted nanodisc by size-exclusion chromatogram (Superose 6 increase). Peak fraction (marked by blue dashed lines) of GlyT1 in digitonin or nanodisc were pooled and concentrated for nanodisc reconstitution or cryo-EM study, respectively.

(E) SDS-PAGE gel of the GlyT1 cryo-EM sample stained with Coomassie blue. Components of the reconstituted nanodisc complex are labeled. The experiments are repeated independently for more than 3 times with similar results.

(F–I) Flowchart for cryo-EM data processing of PF-03463275-bound GlyT1 (GlyT1^{PF}), ALX-5407-bound GlyT1 (GlyT1^{ALX}), SSR504734-bound GlyT1 (GlyT1^{SSR}), and glycine-bound GlyT1 (GlyT1^{Gly}) with final cryo-EM maps colored by local resolution and angular distribution of the particles used in the final reconstruction. Representative raw cryo-EM micrograph and 2D class averages show distinct secondary structure features from different views of each structure (scale bars, 50 nm). Several rounds of classifications are conducted to clean particles, followed by CTF refine and local refine to improve image quality. The final is reported at 3.0, 3.3, 3.1, and 2.6 Å according to the GSFSC (gold standard Fourier ring correlation) criterion. Fourier shell correlations (FSC) of the final map for each structure are calculated between two independently refined half-maps before (blue) and after (red) post-processing. The FSC curve calculated between the cryo-EM density map and the corresponding structural model is shown in black.

(J–M) The cryo-EM density and atomic model of TM1-12 of GlyT1^{PF}, GlyT1^{ALX}, GlyT1^{SSR}, and GlyT1^{Gly} complexes.

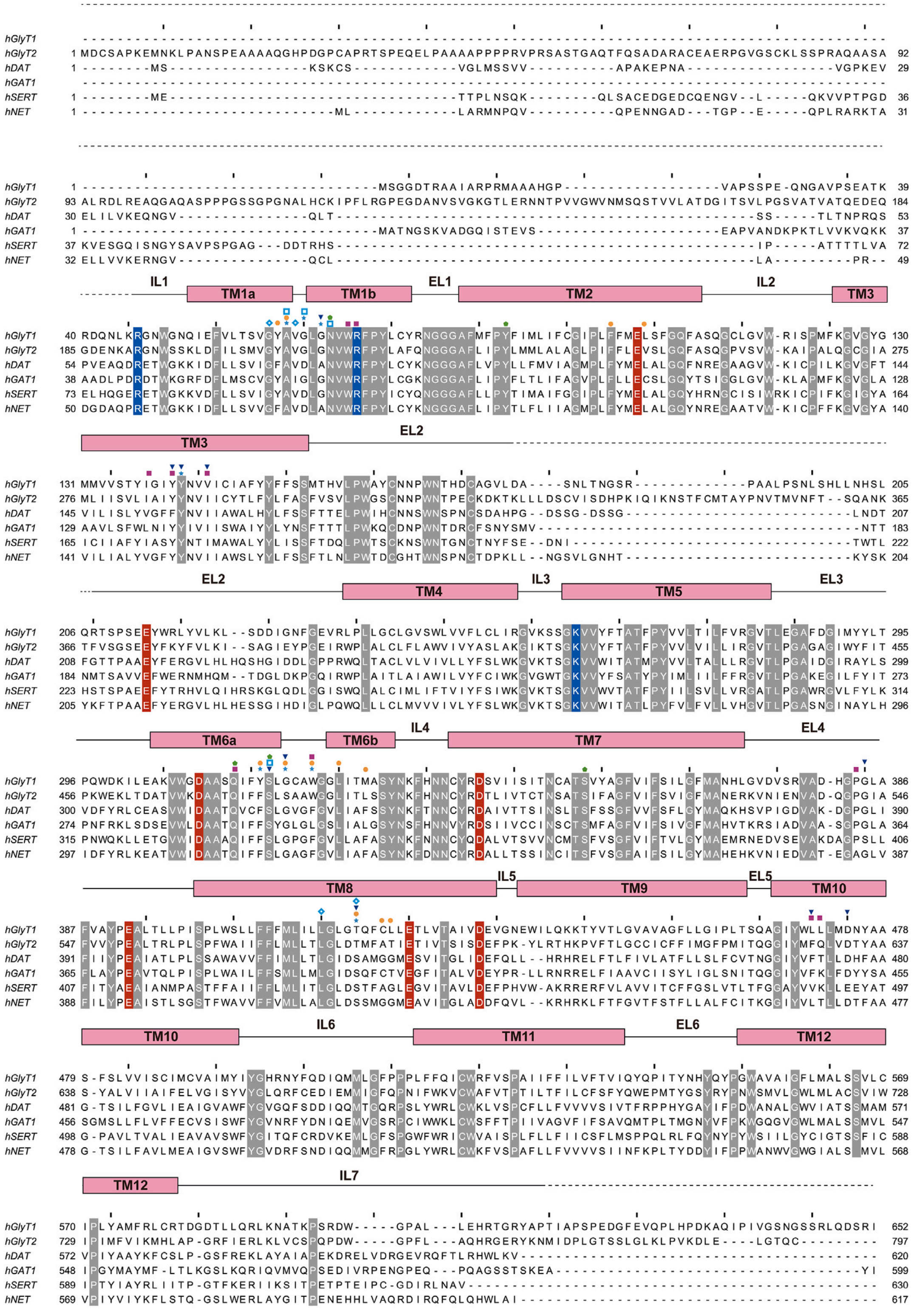

```
hGlyT1       --------------------------------------------------------------------------------------------
hGlyT2     1 MDCSAPKEMNKLPANSPEAAAAQGHPDGPCAPRTSPEQELPAAAAPPPPRVPRSASTGAQTFQSADARACEAERPGVGSCKLSSPRAQAASA  92
hDAT       1 --------MS----------------KSKCS------------VGLMSSVV---------APAKEPNA------------------VGPKEV  29
hGAT1        --------------------------------------------------------------------------------------------
hSERT      1 --------ME---------------------------------TTPLNSQK-------QLSACEDGEDCQENGV--L------QKVVPTPGD  36
hNET       1 ----------------------------ML-------------LARMNPQV---------QPENNGAD---TGP--E------QPLRARKTA  31

hGlyT1     1 ---------------------------------MSGGDTRAAIARPRMAAAHGP-------------------VAPSSPE-QNGAVPSEATK  39
hGlyT2    93 ALRDLREAQGAQASPPPGSSGPGNALHCKIPFLRGPEGDANVSVGKGTLERNNTPVVGWVNMSQSTVVLATDGITSVLPGSVATVATQEDEQ 184
hDAT      30 ELILVKEQNGV---------------QLT------------------------------------------------SS-----TLTNPRQS  53
hGAT1      1 ---------------------------------MATNGSKVADGQISTEVS----------------------EAPVANDKPKTLVVKVQKK  37
hSERT     37 KVESGQISNGYSAVPSPGAG---DDTRHS------------------------------------------------IP-----ATTTTLVA  72
hNET      32 ELLVVKERNGV---------------QCL------------------------------------------------LA---------PR--  49

hGlyT1    40 RDQNLKRGNWGNQIEFVLTSVGYAVGLGNVWRFPYLCYRNGGGAFMFPYFIMLIFCGIPLFFMELSFGQFASQGCLGVW-RISPMFKGVGYG 130
hGlyT2   185 GDENKARGNWSSKLDFILSMVGYAVGLGNVWRFPYLAFQNGGGAFLIPYLMMLALAGLPIFFLEVSLGQFASQGPVSVW-KAIPALQGCGIA 275
hDAT      54 PVEAQDRETWGKKIDFLLSVIGFAVDLANVWRFPYLCYKNGGGAFLVPYLLFMVIAGMPLFYMELALGQFNREGAAGVW-KICPILKGVGFT 144
hGAT1     38 AADLPDRDTWKGRFDFLMSCVGYAIGLGNVWRFPYLCGKNGGGAFLIPYFLTLIFAGVPLFLLECSLGQYTSIGGLGVW-KLAPMFKGVGLA 128
hSERT     73 ELHQGERETWGKKVDFLLSVIGYAVDLGNVWRFPYICYQNGGGAFLLPYTIMAIFGGIPLFYMELALGQYHRNGCISIWRKICPIFKGIGYA 164
hNET      50 DGDAQPRETWGKKIDFLLSVVGFAVDLANVWRFPYLCYKNGGGAFLIPYTLFLIIAGMPLFYMELALGQYNREGAATVW-KICPFFKGVGYA 140

hGlyT1   131 MMVVSTYIGIYYNVVICIAFYYFFSSMTHVLPWAYCNNPWNTHDCAGVLDA---SNLTNGSR--------------PAALPSNLSHLLNHSL 205
hGlyT2   276 MLIISVLIAIYYNVIICYTLFYLFASFVSVLPWGSCNNPWNTPECKDKTKLLLDSCVISDHPKIQIKNSTFCMTAYPNVTMVNFT--SQANK 365
hDAT     145 VILISLYVGFFYNVIIAWALHYLFSSFTTELPWIHCNNSWNSPNCSDAHPG--DSSG-DSSG--------------------------LNDT 207
hGAT1    129 AAVLSFWLNIYYIVIISWAIYYLYNSFTTTLPWKQCDNPWNTDRCFSNYSMV-------------------------------------NTT 183
hSERT    165 ICIIAFYIASYYNTIMAWALYYLISSFTDQLPWTSCKNSWNTGNCTNYFSE--DNI--------------------------------TWTL 222
hNET     141 VILIALYVGFYYNVIIAWSLYYLFSSFTLNLPWTDCGHTWNSPNCTDPKLL--NGSVLGNHT--------------------------KYSK 204

hGlyT1   206 QRTSPSEEYWRLYVLKL--SDDIGNFGEVRLPLLGCLGVSWLVVFLCLIRGVKSSGKVVYFTATFPYVVLTILFVRGVTLEGAFDGIMYYLT 295
hGlyT2   366 TFVSGSEEYFKYFVLKI--SAGIEYPGEIRWPLALCLFLAWVIVYASLAKGIKTSGKVVYFTATFPYVVLVILLIRGVTLPGAGAGIWYFIT 455
hDAT     208 FGTTPAAEYFERGVLHLHQSHGIDDLGPPRWQLTACLVLVIVLLYFSLWKGVKTSGKVVWITATMPYVVLTALLLRGVTLPGAIDGIRAYLS 299
hGAT1    184 NMTSAVVEFWERNMHQM--TDGLDKPGQIRWPLAITLAIAWILVYFCIWKGVGWTGKVVYFSATYPYIMLIILFFRGVTLPGAKEGILFYIT 273
hSERT    223 HSTSPAEEFYTRHVLQIHRSKGLQDLGGISWQLALCIMLIFTVIYFSIWKGVKTSGKVVWVTATFPYIILSVLLVRGATLPGAWRGVLFYLK 314
hNET     205 YKFTPAAEFYERGVLHLHESSGIHDIGLPQWQLLLCLMVVVIVLYFSLWKGVKTSGKVVWITATLPYFVLFVLLVHGVTLPGASNGINAYLH 296

hGlyT1   296 PQWDKILEAKVWGDAASQIFYSLGCAWGGLITMASYNKFHNNCYRDSVIISITNCATSVYAGFVIFSILGFMANHLGVDVSRVAD-HGPGLA 386
hGlyT2   456 PKWEKLTDATVWKDAATQIFFSLSAAWGGLITLSSYNKFHNNCYRDTLIVTCTNSATSIFAGFVIFSVIGFMANERKVNIENVAD-QGPGIA 546
hDAT     300 VDFYRLCEASVWIDAATQVCFSLGVGFGVLIAFSSYNKFTNNCYRDAIVTTSINSLTSFSSGFVVFSFLGYMAQKHSVPIGDVAK-DGPGLI 390
hGAT1    274 PNFRKLSDSEVWLDAATQIFFSYGLGLGSLIALGSYNSFHNNVYRDSIIVCCINSCTSMFAGFVIFSIVGFMAHVTKRSIADVAA-SGPGLA 364
hSERT    315 PNWQKLLETGVWIDAAAQIFFSLGPGFGVLLAFASYNKFNNNCYQDALVTSVVNCMTSFVSGFVIFTVLGYMAEMRNEDVSEVAKDAGPSLL 406
hNET     297 IDFYRLKEATVWIDAATQIFFSLGAGFGVLIAFASYNKFDNNCYRDALLTSSINCITSFVSGFAIFSILGYMAHEHKVNIEDVAT-EGAGLV 387

hGlyT1   387 FVAYPEALTLLPISPLWSLLFFFMLILLGLGTQFCLLETLVTAIVDEVGNEWILQKKTYVTLGVAVAGFLLGIPLTSQAGIYWLLLMDNYAA 478
hGlyT2   547 FVVYPEALTRLPLSPFWAIIFFLMLTLGLDTMFATIETIVTSISDEFPK-YLRTHKPVFTLGCCICFFIMGFPMITQGGIYMFQLVDTYAA 637
hDAT     391 FIIYPEAIATLPLSSAWAVVFFIMLLTLGIDSAMGGMESVITGLIDEFQLL--HRHRELFTLFIVLATFLLSLFCVTNGGIYVFTLLDHFAA 480
hGAT1    365 FLAYPEAVTQLPISPLWAILFFSMLLMLGIDSQFCTVEGFITALVDEYPR-LLRNRRELFIAAVCIISYLIGLSNITQGGIYVFKLFDYYSA 455
hSERT    407 FITYAEAIANMPASTFFAIIFFLMLITLGLDSTFAGLEGVITAVLDEFPHVW-AKRRERFVLAVVITCFFGSLVTLTFGGAYVVKLLEEYAT 497
hNET     388 FILYPEAISTLSGSTFWAVVFFVMLLALGLDSSMGGMEAVITGLADDFQVL--KRHRKLFTFGVTFSTFLLALFCITKGGIYVLTLLDTFAA 477

hGlyT1   479 S-FSLVVISCIMCVAIMYIYGHRNYFQDIQMMLGFPPPLFFQICWRFVSPAIIFFILVFTVIQYQPITYNHYQYPGWAVAIGFLMALSSVLC 569
hGlyT2   638 S-YALVIIAIFELVGISYVYGLQRFCEDIEMMIGFQPNIFWKVCWAFVTPTILTFILCFSFYQWEPMTYGSYRYPNWSMVLGWLMLACSVIW 728
hDAT     481 G-TSILFGVLIEAIGVAWFYGVGQFSDDIQQMTGQRPSLYWRLCWKLVSPCFLLFVVVVSIVTFRPPHYGAYIFPDWANALGWVIATSSMAM 571
hGAT1    456 SGMSLLFLVFFECVSISWFYGVNRFYDNIQEMVGSRPCIWWKLCWSFFTPIIVAGVFIFSAVQMTPLTMGNYVFPKWGQGVGWLMALSSMVL 547
hSERT    498 G-PAVLTVALIEAVAVSWFYGITQFCRDVKEMLGFSPGWFWRICWVAISPLFLLFIICSFLMSPPQLRLFQYNYPYWSIILGYCIGTSSFIC 588
hNET     478 G-TSILFAVLMEAIGVSWFYGVDRFSNDIQQMMGFRPGLYWRLCWKFVSPAFLLFVVVVSIINFKPLTYDDYIFPPWANWVGWGIALS MVL 568

hGlyT1   570 IPLYAMFRLCRTDGDTLLQRLKNATKPSRDW-----GPAL---LEHRTGRYAPTIAPSPEDGFEVQPLHPDKAQIPIVGSNGSSRLQDSRI 652
hGlyT2   729 IPIMFVIKMHLAP-GRFIERLKLVCSPQPDW-----GPFL---AQHRGERYKNMIDPLGTSSLGLKLPVKDLE----LGTQC--------- 797
hDAT     572 VPIYAAYKFCSLP-GSFREKLAYAIAPEKDRELVDRGEVRQFTLRHWLKV----------------------------------------- 620
hGAT1    548 IPGYMAYMF-LTLKGSLKQRIQVMVQPSEDIVRPENGPEQ---PQAGSSTSKEA-----------------------------------YI 599
hSERT    589 IPTYIAYRLIITP-GTFKERIIKSITPETPTEIPC-GDIRLNAV----------------------------------------------- 630
hNET     569 VPIYVIYKFLSTQ-GSLWERLAYGITPENEHHLVAQRDIRQFQLQHWLAI----------------------------------------- 617
```

Symbol of Binding Sites ★ **Glycine** ● **ALX-5407** ■ **SSR504734** ▼ **PF-03463275** □ **Na1** ◇ **Na2** ⬟ **Cl**

(legend on next page)

Figure S2. Sequence alignment of human neurotransmitter transporters, related to Figures 2, 3, 4, and 6

Secondary structural elements of human glycine transporter 1 (hGlyT1, *SLC6A9*, and UniProt: P48067-3) are depicted above the sequence alignment, and unmodeled loops are represented as dashed lines. Human glycine transporter 2 (hGlyT2, *SLC6A5*, and UniProt: Q9Y345-1), human dopamine transporter (hDAT, *SLC6A3*, and UniProt: Q01959-1), human GABA transporter 1 (hGAT1, *SLC6A1*, and UniProt: P30531-1), human serotonin transporter (hSERT, *SLC6A4*, and UniProt: P31645-1), and human noradrenaline transporter (hNET, *SLC6A2*, and UniProt: P23975-1) are aligned with human glycine transporter 1 by the Clustal Omega program and formatted with Jalview. Conservative residues among these proteins are highlighted in red, blue, and gray for acidic, basic, and others, respectively. The residues contributed to ligands binding are labeled by different symbols above residues.

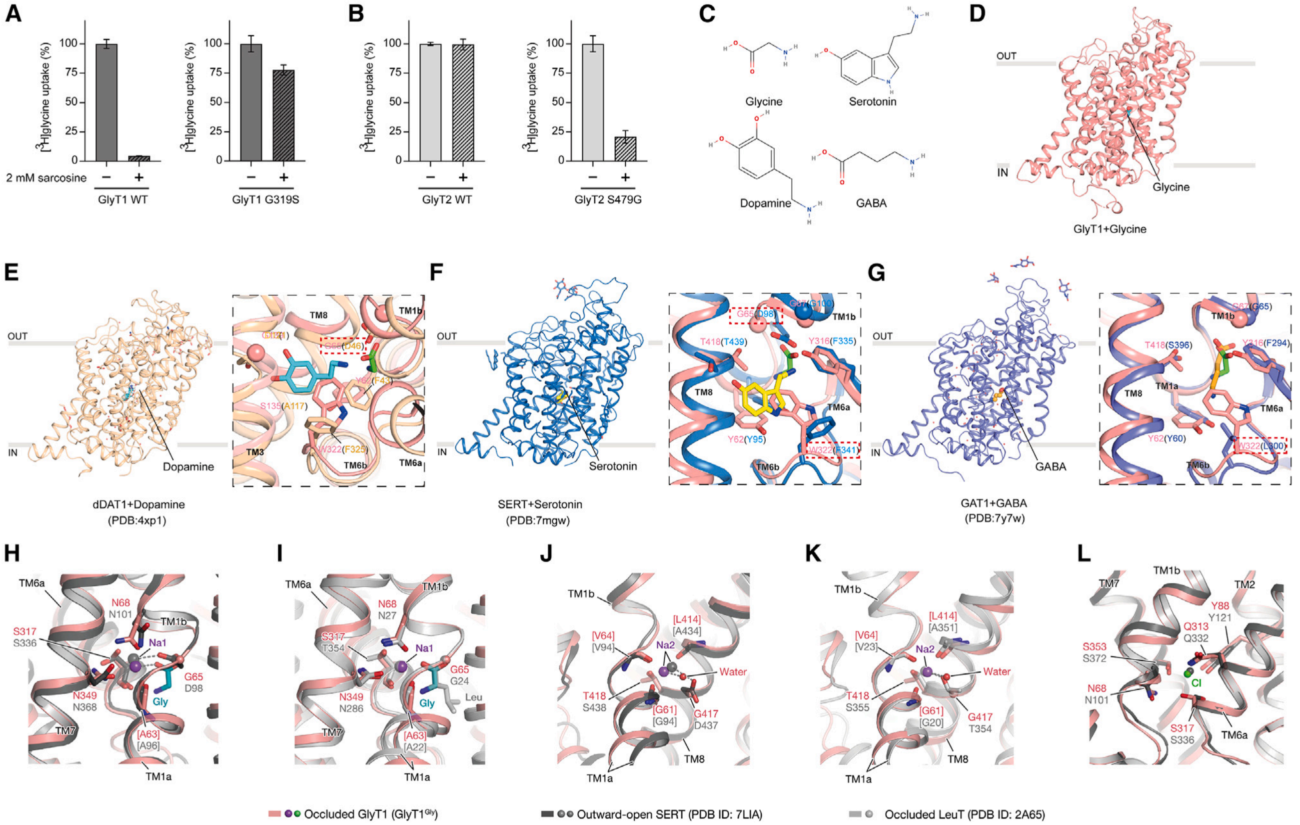

Figure S3. Selectivity of substrate-binding pockets in GlyT1, dDAT, SERT, and GAT1 and comparison of ion binding sites in GlyT1, SERT, and LeuT, related to Figure 2

(A and B) The transport activities of WT GlyT1, GlyT1 mutant G319S, WT GlyT2, and GlyT2 mutant S479G were assessed using a $[^3H]$glycine uptake assay, both in the absence and presence of 2 mM sarcosine. The results were normalized to the transport activity of each construct under conditions without sarcosine. Data are shown as mean ± SEM (error bars); n = 3 biologically independent samples.

(C) The chemical structure of glycine, dopamine, serotonin, and GABA were displayed.

(D) The glycine-bound GlyT1, dopamine-bound dDAT (PDB: 4XP1), serotonin-bound SERT (PDB: 7MGW), and GABA-bound GAT1 (PDB: 7Y7W) are represented by salmon, wheat, marine, and violet cartoon, respectively. The substrates glycine, dopamine, serotonin, and GABA are represented by green, cyan, yellow, and orange sphere, respectively.

(E–G) Comparison of glycine binding pocket and dopamine/serotonin/GABA binding pocket. The key residues of GlyT1, dDAT, SERT, and GAT1 are represented by sticks and labeled. Glycine, dopamine, serotonin, and GABA molecules are represented by green, cyan, yellow, and orange sticks, respectively.

(H–L) Superposition of Na1 (H and I), Na2 (J and K), and Cl (L) binding site among GlyT1^{Gly} (salmon), SERT (black, PDB: 7LIA), and LeuT (gray, PDB: 2A65). Sodium ions are shown as purple (Na1 and Na2 in GlyT1), black (Na1 and Na2 in SERT), and gray (Na1 and Na2 in LeuT) spheres, respectively. Chloride ions are displayed as green (in GlyT1) and gray (in LeuT) spheres, respectively. Waters involved in interactions are shown as red spheres. Glycine (Gly) and leucine (Leu) are represented as cyan and gray sticks, respectively. Residues that participate in the interaction via backbone atoms are labeled with square brackets. Different hydrogen bonds interactions among GlyT1, SERT, and LeuT are depicted via dashed line.

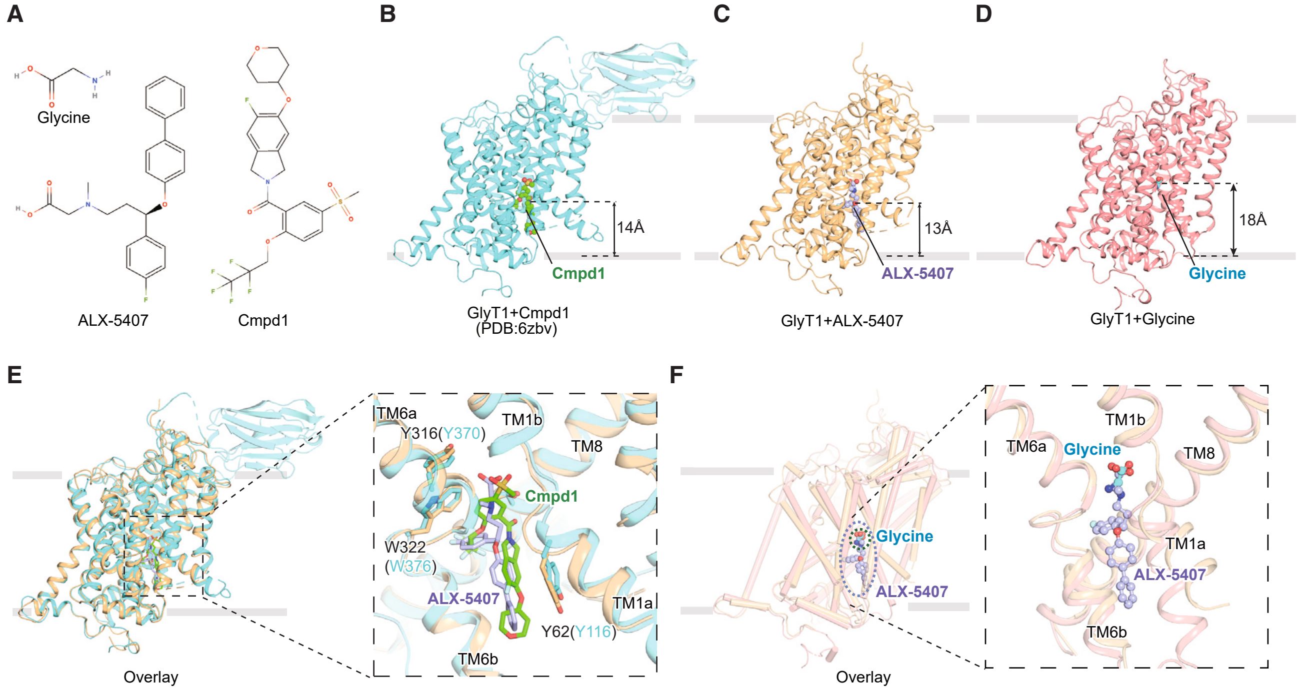

Figure S4. Comparison of binding sites of ALX-5407, glycine, and Cmpd1, related to Figure 3

(A) The chemical structures of ALX-5407, glycine, and Cmpd1 are depicted.

(B–D) Inward-open Cmpd1 bound GlyT1 (GlyT1^{Cmpd1}, PDB: 6ZBV), ALX-5407 bound GlyT1 (GlyT1^{ALX}), and glycine-bound GlyT1 (GlyT1^{Gly}) are represented by cyan, light-orange, and salmon cartoon, respectively. Cmpd1, ALX-5407, and glycine are displayed by green, light-purple, and cyan spheres and labeled, respectively.

(E) GlyT1^{Cmpd1} and GlyT1^{ALX} are aligned and overlaid. (Inset) The Cmpd1 and ALX-5407 molecules are represented by green and light-purple sticks, respectively. The key residues are represented by sticks both in GlyT1^{Cmpd1} and GlyT1^{ALX} and labeled by different colors.

(F) GlyT1^{Gly} (salmon) and GlyT1^{ALX} (light-orange) are aligned. Glycine and ALX-5407 are represented by cyan and light-purple stick, respectively. The extended panel depicted the detailed comparison of glycine and ALX-5407 binding sites.

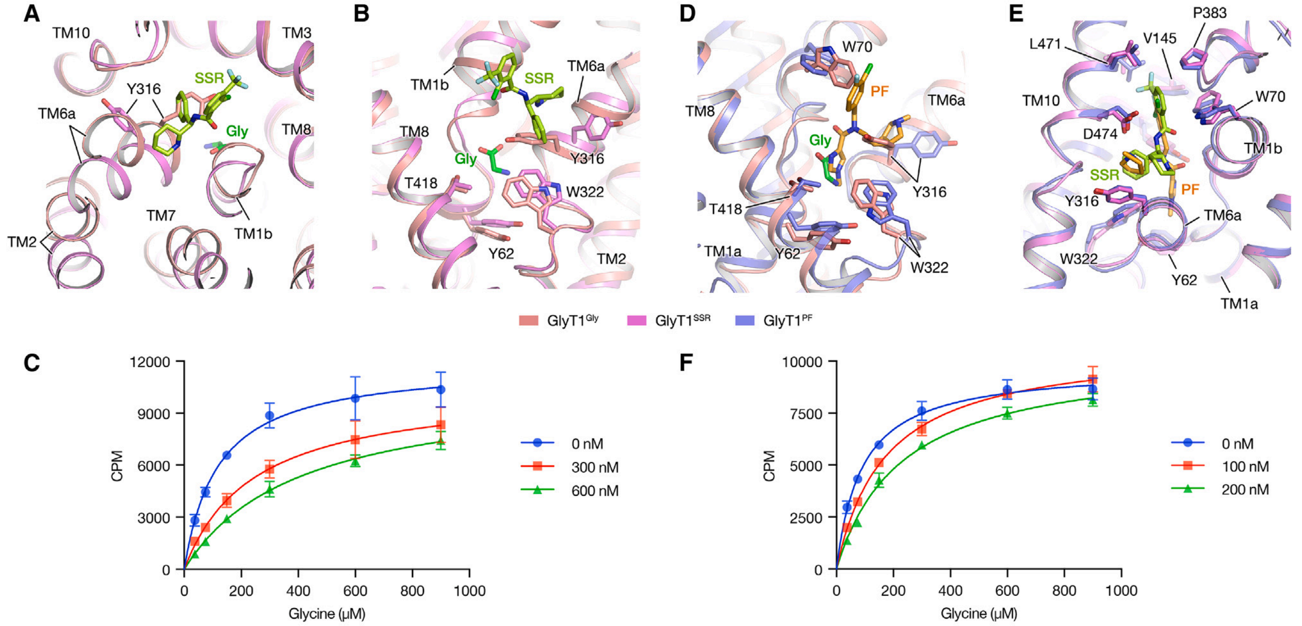

SSR504734 (nM)	0	300	600
V_{max} (CPM)	12085 ± 1583	10617 ± 1688	10737 ± 1111
K_m (μM)	125.3 ± 32.65	243.3 ± 32.99	406.7 ± 47.47

PF-03463275 (nM)	0	100	200
V_{max} (CPM)	9793 ± 707	11045 ± 884	10415 ± 335
K_m (μM)	92.74 ± 18.7	184.5 ± 41.2	235.9 ± 26.7

Figure S5. Mechanism of competitive inhibition of SSR504734 and PF-03463475, related to Figures 4 and 6

(A and B) Superposition of GlyT1^{SSR} (pink cartoon) and GlyT1^{Gly} (salmon cartoon). RMSD value is calculated as 1.8 Å over 488 Cα atoms. SSR504734 and glycine are depicted as lemon and green sticks, respectively. Key residues are showed as sticks.

(C) Plots of [^{3}H]glycine uptake by GlyT1 in the absence (0 nM in blue) or presence (300 nM in red and 600 nM in green) of SSR504734. Data in curve are obtained from three biologically independent experiments and are presented as mean ± SEM (error bars). The resulting kinetic parameters, including V_{max} and K_m, shown in table represent mean ± SEM. In the presence of SSR504734, there is no significant difference in V_{max} values compared with WT GlyT1 ($p = 0.7203$ for 300 nM SSR504734 group, $p = 0.7557$ for 600 nM SSR504734 group). Although the K_m value for the 300 nM SSR504734 group is not significantly different from WT GlyT1 ($p = 0.1228$), the 600 nM SSR504734 group displays a significant difference ($p = 0.0037$). Statistical comparisons were conducted using one-way ANOVA followed by Dunnett's test to determine significant differences.

(D and E) The binding site of PF-03463275 (orange sticks) compared with SSR504734 (light-green sticks) and glycine (green sticks). The models of GlyT1^{PF}, GlyT1^{SSR}, and GlyT1^{Gly} are represented by blue, purple, and salmon cartoon, respectively. The key residues involved in interaction are showed as sticks.

(F) Plots of [^{3}H]glycine uptake by GlyT1 in the absence (0 nM in blue) or presence (100 nM in red and 200 nM in green) of PF-03463275. Data points in curve are presented as mean ± SEM (error bars); n = 3 biologically independent samples. The resulting kinetic parameters, including V_{max} and K_m, shown in table represent mean ± SEM. In the presence of PF-03463275, there is no significant difference in V_{max} values compared with WT GlyT1 ($p = 0.3828$ for 100 nM PF-03463275 group, $p = 0.7542$ for 200 nM PF-03463275 group). Although the K_m value for the 100 nM PF-03463275 group is not significantly different from WT GlyT1 ($p = 0.1289$), the 200 nM PF-03463275 group displays a significant difference ($p = 0.0275$). Statistical comparisons were conducted using one-way ANOVA followed by Dunnett's test to determine significant differences.

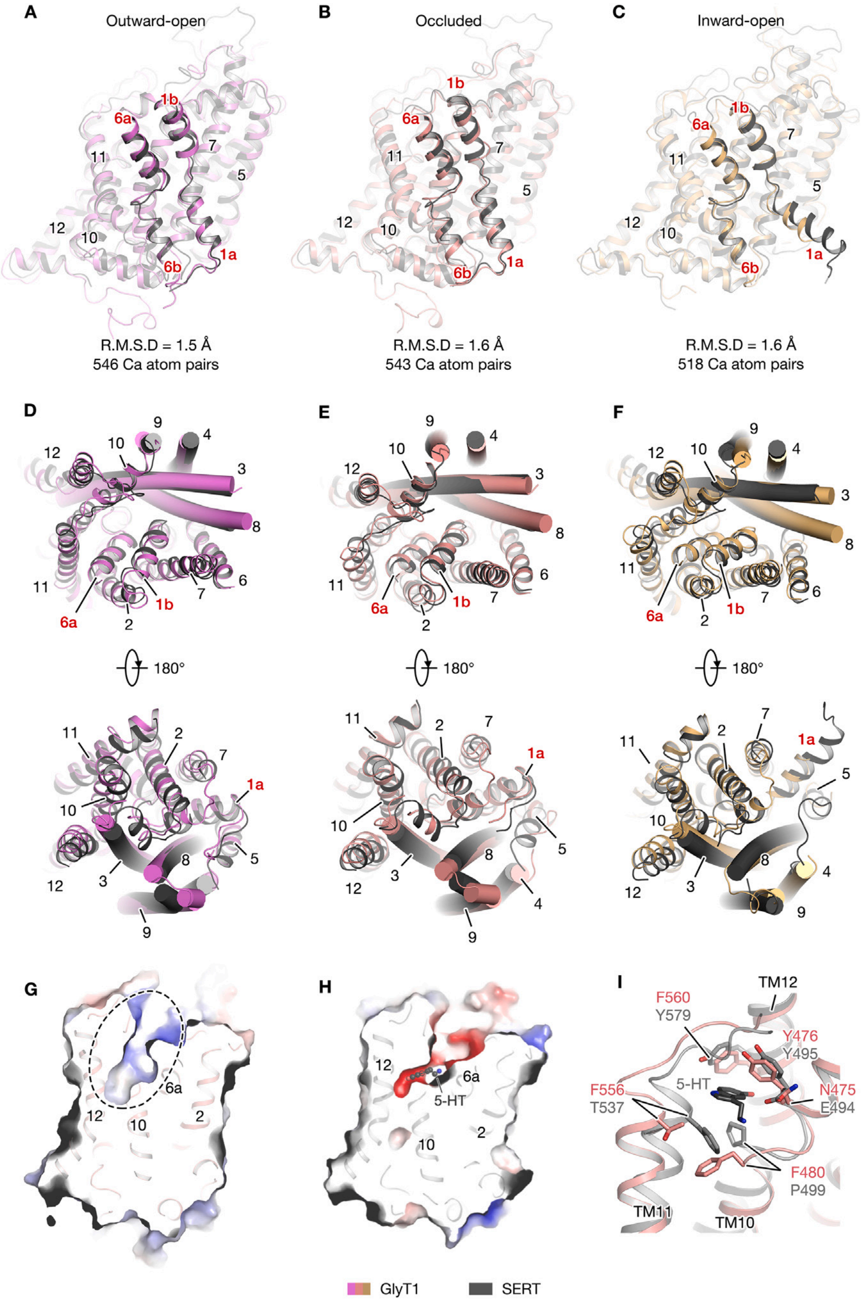

Figure S6. Comparison of three different conformational states between GlyT1 and SERT, related to Figures 2, 3, 4, and 5

(A–C) Overall alignment of GlyT1 and SERT in the outward-open, occluded, and inward-open conformations. GlyT1 in the outward-open, occluded, and inward-open state is colored purple, salmon, and yellow, respectively. SERT is colored black in all three states (PDB: 6DZY, 7MGW, and 6DZZ). Helices that participate in conformational changes are highlighted with red labels.

(D–F) Superposition of "top-down" (up) and "bottom-up" (down) views of outward-open (D), occluded (E), and inward-open states (F) of GlyT1 and SERT using scaffold helices (TM3, TM4, TM8, and TM9 shown as cylinders) as alignment reference. Helices that participate in conformational changes are highlighted with red labels.

(G) Surface electrostatic potential map of the occluded states of GlyT1, a cavity is observed in the site circled by dash line.

(H) Surface electrostatic potential map of the occluded state of SERT. Serotonin (5-HT) is displayed as black spheres and sticks and accommodated in the allosteric binding site (S2) of SERT.

(I) Comparison of the allosteric binding site in SERT and the corresponding site in GlyT1. Residues involved in the interactions between 5-HT and the allosteric binding site of SERT are shown as black sticks. Corresponding residues in GlyT1 are shown as salmon sticks.